Volume 1 | Number 1 | Jan 2013 | Pages 1–100

Journal of
Materials Chemistry A

Materials for energy and sustainability
www.rsc.org/materialsA

Li⁺

ROYAL SOCIETY
OF CHEMISTRY

ROYAL SOCIETY
OF **CHEMISTRY**

www.rsc.org/materialsA

Recent advances and progress in the development of graphene-based adsorbents for CO₂ capture

Rajasekhar Balasubramanian*, Shamik Chowdhury

Department of Civil & Environmental Engineering,National University of Singapore, 1 Engineering Drive 2, Singapore 117576, Republic of Singapore

_____

* Corresponding author. E-mail: ceerbala@nus.edu.sg

Fax: +65 67744202; Tel.: +65 65165135.

Abstract

With the current high consumption of fossil fuels and the rapid increase in atmospheric CO_2 concentrations, there is a strong need for energy efficient and selective capture of CO_2 from fossil-fuelled power plants and other large industrial sources. Among the various adsorbents explored by the scientific community for CO_2 removal from flue gases, graphene is receiving increased attention because of its unique molecular structure and many exciting properties such as high mechanical strength, excellent thermal conductivity, good chemical stability, large accessible surface area, and tunable porosity. In addition, the facile surface functionalization of graphene leads to production of innovative graphene-based materials that have the potential to be applied as advanced next-generation CO_2 adsorbents. As a consequence, graphene and its derivatives has been the subject of intense experimental investigations and theoretical studies, probing their unmatched structural versatility for CO_2 abatement. This review aims at bringing together the latest developments in the rapidly evolving cross-disciplinary field of graphene-mediated CO_2 adsorption. In addition, it provides new research directions for making further advances toward practical deployment of graphene-based CO_2 adsorbents.

Table of contents
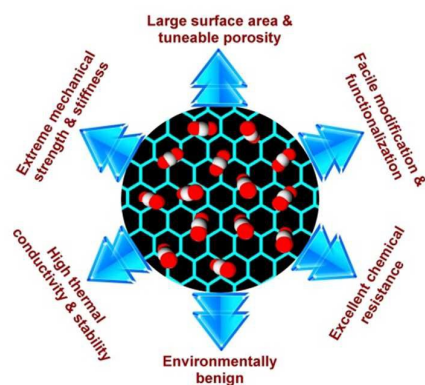
Review of recent advances in graphene-mediated CO_2 adsorption from flue gases, a rapidly evolving cross-disciplinary field of current global interest.

About the authors

Rajasekhar Balasubramanian

Rajasekhar Balasubramanianis an Associate Professor in the Department of Civil and Environmental Engineering at the National University of Singapore. He received his PhD in Atmospheric Chemistry from the University of Miami, USA in 1991 and has research experience and interests ranging across: Air Quality, Climate Change, Aerosol Science & Technology, Health Risk Assessment, and Development of Environmental Remediation Technologies. He has authored more than 200 refereed publications. In recognition of his outstanding contributions in Environmental Science & Engineering, he has been honored with numerous awards including the Alan Berman Research Publication Award from the US Department of Navy in 2014.

Shamik Chowdhury

Shamik Chowdhurywas born in the Indian state of West Bengal in 1987. He earned his BTech (2009) from West Bengal University of Technology, India and MTech (Gold Medalist) (2011) from National Institute of Technology Durgapur, India, both in Biotechnology. He then joined Prof. Rajasekhar Balasubramanian's group at the National University of Singapore as a PhD candidate. His main research interests include the development of functional nanomaterials, especially graphene-based composite systems for environmental remediation. Currently, his is focused on the design and synthesis of novel graphene-based structures and their application in gas separation and storage.

1.Introduction

Atmospheric CO_2 concentrations continue to rise rapidly in response to increased combustion of fossil fuels, especially coal, to meet the world's growing energy demand. Because CO_2 is a major greenhouse gas contributing to global climate change, a rapid transition to a sustainable low carbon energy system has become an absolute necessity. However, coal is still affordable, reliable and abundantly available.[1] Many countries have huge coal reserves within their geographical borders, and are therefore unlikely to reduce their reliance on this fossil fuel in the short- and intermediate-term.[2] Moreover, between now and 2050, the world economy is projected to rise exponentially in the emerging and developing nations.[3] Such rapid economic growth will inevitably require increased energy consumption, much of which would likely come from coal. As a consequence, mitigation of CO_2 emissions from coal and other fossil fuel-fired power plants is of increased concern from the climate change viewpoint.

There is a widespread consensus that the selective removal of CO_2 from flue gases, followed by its compression and subsequent sequestration in deep underground geologic formations, can effectively reduce the carbon footprint of existing power plants.[4,5] The importance of such carbon capture and storage (CCS) as a short/medium-term technological option to curb anthropogenic energy-related CO_2 emissions has been globally recognized.[6,7] However, despite extensive research on CO_2 capture from flue gases, progress in deploying CCS-based technologies has been impeded mainly due to technical difficulties in the efficient extraction of CO_2 from the exhaust of coal-fired power plants and expensive operations associated with this separation process.[8] Hence, there is an urgent need to develop efficient CO_2 capture techniques, such as those potentially offered by solid adsorbents, to achieve a secure, cost-effective and low-carbon electricity supply for the foreseeable future.[9, 10]

Among the various solid adsorbents that are currently being explored for capturing CO_2 emanating from fossil fuel combustion systems, graphene, a novel two dimensional (2D) nanomaterial with a wide range of intriguing characteristics, is receiving considerable attention.[11] Indeed, substantial scientific progress has been made in recent years in terms of evaluating the performance of graphene and its derivatives as adsorbents for selective separation of CO_2 under different flue gas conditions. At the same time, there remain a range of technical challenges that need to be overcome in order to make graphene-based materials as next-generation CO_2 adsorbents. This review brings together the current knowledge available in the literature in the development of graphene-based CO_2 adsorbents, identifies key knowledge gaps, and provides new strategic research directions toward the use of graphene-based CO_2 adsorbents for large-scale industrial applications. To the best of our knowledge, this is the first comprehensive review of its kind in the rapidly evolving cross-disciplinary field of graphene-mediated CO_2 adsorption.

2.Current status of CO_2 capture technologies

Efficient capture of CO_2 from large point sources of air pollution is a top global priority for stabilizing the CO_2 level in the atmosphere. This goal can be achieved by adopting one of the following three strategies (Fig. 1): (1) pre-combustion capture, where the carbon content of the fuel is stripped off prior to combustion by reacting it with steam (known as 'steam reforming') or oxygen (known as 'partial oxidation' or 'gasification'), producing a syngas composed mainly of CO and H_2 which is then subsequently reacted with steam (through a water-gas shift reaction), thereby generating additional H_2 and oxidizing CO to CO_2; (2) post-combustion capture, where CO_2 is removed from a flue gas resulting from the burning of fossil fuels in ambient air; and (3) oxyfuel-combustion systems, where the combustion is performed in pure oxygen instead of air leading to a flue gas that primarily consists of CO_2

6

and H_2O.[12-14] Among the three approaches, oxyfuel-combustion is a near-zero emission technology for both new and existing pulverized fossil-fired power stations.[15] However, oxy combustion options are still under development and will require significantly more effort to reach operational and commercial readiness.[16] On the contrary, both pre-combustion and post-combustion capture is technically feasible and has the potential to reduce CO_2 emissions by a gigaton or more per year.[17] Table 1 summarizes the typical composition and physical condition of flue gas streams relevant to pre- and post-combustion CO_2 capture processes. Evidently, each of these capture scenarios entails different gas separation requirements and constraints mainly due to variations in the flue gas composition and operating environment as well as inconsistency in physical properties (i.e., effective kinetic diameter, dipole moment, quadrupole moment and polarization) of the gases involved (see Table 2). For example, in pre-combustion capture, a concentrated, high-pressure, and hot CO_2/H_2 mixture has to be treated where the difference in polarizability between the gases is considerably large whereas in post-combustion capture, a diluted, low-pressure, and wet CO_2/N_2 mixture has to be treated where the difference in effective kinetic diameter between the gases is relatively small. Accordingly, several technologies with varying degrees of maturity have been proposed for CO_2 capture from both concentrated and dilute gas mixtures, including absorption, adsorption, and membrane separation.[18,22,23] While chemical absorption with alkanolamines (or variants) can inflict a parasitic energy penalty on top of the energy produced by the power plant,[24] most membrane-based gas separation methods are still in their infancy.[25] Adsorption, on the other hand, is an attractive option to curb CO_2 emissions because of its comparatively less energy requirements and many other competitive advantages (including simplicity of operation, applicability over a relatively wide range of temperature and pressure conditions, and low capital investment costs).[26,27]

Adsorption technologies use solid adsorbents that allow selective removal of CO_2 from various constituents of the flue gas mixture because of different interaction forces between the gases and the solid surface. Depending on the type of adsorbent used, CO_2 is adsorbed by either weak attraction forces such as electrostatic or van der Waals forces (physisorption) or through strong chemical bonds (chemisorption).[28] These adsorbents are usually employed in a cyclic procedure that alternate between adsorption and desorption modes of operation, with desorption induced by increasing the temperature (temperature swing adsorption (TSA)), reducing the pressure (pressure swing adsorption (PSA)), or by creating a near-vacuum (vacuum swing adsorption (VSA)).[29] Since in pre-combustion capture the gas stream is inherently pressurized after the conversion reactions, a PSA process is the most suitable. On the other hand, in post-combustion capture the flue gas is released at near ambient pressure. Compressing or applying a vacuum to such a large volume of gas is difficult, a TSA cycle is therefore the most appropriate.[30] Nevertheless, regardless of the regeneration method, almost pure CO_2 can be recovered for subsequent sequestration. For adsorption-based gas separations to attain commercial viability, one of the main challenges is the development of suitable adsorbents that satisfy the performance standards for deployment in coal- and natural gas-fired power plants. As described in Table 3, effective adsorbents for carbon capture must possess the following key features: (i) high adsorption capacity, (ii) high selectivity, (iii) moderate heat of adsorption, (iv) fast adsorption and desorption kinetics, and (v) excellent chemical and mechanical stability. These operational criteria should also be finely tuned depending on the type of CO_2 capture to be performed (i.e., pre-combustion or post-combustion) and the specific configuration of the power plant (which depends on the type of fuel being burned in that particular plant). Recently, a variety of solid adsorbents have been studied comprehensively for CO_2 capture, such as zeolites, porous silica, metal oxides, porous polymers, alumina, activated carbon, carbon fibers, ion-exchange resin, and metal

organic frameworks (MOF).[9,19,35-43] Some of them have low adsorption capacities and/or require long time to reach saturation due to slow adsorption kinetics, or sometimes poor selectivity relative to other gases.[43] Furthermore, most of these adsorbents exhibit reduced activity in the presence of moisture, low chemical and thermal stability, or weak mechanical properties that lessen their suitability for on-site application.[43] There is therefore a pressing need to develop advanced solid adsorbents that can adequately address the inherent requirements of real-world capture systems.

3. Graphene as next-generation CO_2 adsorbents

Since its first isolation in 2004, graphene, a carbon monolayer packed into a honeycomb lattice, has proved itself as an exciting material with a wide range of opportunities for new scientific knowledge generation and technological innovations (Fig. 2).[44-46] Graphene already holds tremendous promise for diverse applications: supercapacitors,[47,48] energy storage,[49-50] catalysis,[52] photocatalysis,[53] solar cells,[54] sensing platforms,[55] memory devices,[56] molecular imaging,[57] 3D printing,[58] tissue engineering,[59] drug delivery,[60] water filtration and desalination,[61,62] gas separation and storage,[63,64] sensors for detection of pollutants,[65,66] and remediation of air and water,[67-71] etc. The latest addition to this list is the use of graphene for CO_2 adsorption. Research is conducted to provide answers to questions such as (1) would graphene be able to significantly outperform the state-of-the-art adsorbents that are currently known for CO_2 removal ? (2) is graphene versatile enough to comply with CCS industry standards ? With its amazingly attractive properties, graphene certainly has the potential to be a selective and efficient adsorbent for CO_2 capture if its molecular architecture can be rationally tailored for this application.

Graphene is a strictly 2D material with exceptionally high specific surface area (theoretical value of 2630 $m^2 g^{-1}$).[72] Interestingly, by strategically removing atoms from its hexagonal

lattice to create pores with radii large enough to admit CO_2, adsorbents with concomitantly high CO_2 selectivity and high CO_2 capacity can be developed.[73] These characteristics of graphene make it more attractive compared to the conventional CO_2 adsorbents. In addition, graphene's planar geometry makes it amenable for modification or functionalization,[74] providing essentially infinite possibilities to fabricate adsorbents with properties that are precisely tuned for the desired capture setting.

With respect to large-scale industrial capture of CO_2, one of the defining features of graphene is its inherent mechanical strength and stiffness. Conventional TSA/PSA processes rely on compact packing of adsorbent particles inside an adsorption column in the form of packed beds for continuous operation. Such high-density packing could cause a collapse of the pores and eventually reduce the adsorbent's effective surface area.[75] Additionally, operation with rapid swings in temperature/pressure can lead to mechanical attrition of the adsorbent, causing a host of operational problems that affect the overall performance of the CO_2 capture system.[75] To overcome those technological challenges, adsorbent materials with excellent mechanical stability are currently sought by both academic and industrial communities. Due to the strong in-plane C−C bonds, graphene has an enormous tensile strength of 130 GPa and an exceedingly large Young's modulus of about 1 TPa, making it 30 times harder than diamonds and 200 times harder than steel.[76] Such mechanical properties of graphene are therefore not only attractive for the development of robust adsorbents that can afford high packing densities, but also warrant a long lifetime with a high number of operating cycles. Also, graphene manifests an extraordinary thermal conductivity of up to 5000 W m^{-1} K^{-1}, which stems from its highly anisotropic nature and the low mass of the carbon atoms.[77] For TSA-based CO_2 capture, the impressive thermal conductivity of graphene would ensure a high rate of heat transfer through the adsorbent bed, which would in turn reduce the duration of the regeneration cycle and, lower the operating costs. More importantly, graphene is

chemically inert and relatively stable under conditions where most other substances would undergo rapid phase transition and chemical reactions.[78] This makes graphene extremely favorable for CO_2 capture applications, especially post-combustion capture where substantial quantities of water and other contaminants (O_2, SO_2, NO_x) in the flue gas stream can compromise the long-term stability of the adsorbent. Above all, graphene is environmentally benign and can be easily manufactured by either top down (such as exfoliation from bulk) or bottom up (atom by atom growth) techniques.[79-82]

Because of these unparalleled attributes, graphene is undoubtedly an appealing material for CO_2 sequestration. The unique combination of graphene's structural, chemical, mechanical, and thermal properties enables it to be used as an important building block for next-generation of CO_2 adsorbents, which can overcome the shortcomings of the existing ones. Consequently, there has been an enormous effort in recent years to explore graphene and its oxygen-containing analogue, graphene oxide (GO), for CO_2 capture applications from both the theoretical and experimental scientific communities. This has led to numerous conceptual and practical developments as discussed in the following section.

4.CO_2 adsorption on graphene-based materials

4.2. Experimental exploration and developments

Experimental exploration is the most direct and accurate means of determining the adsorption characteristics of any material, and is a prerequisite for the assessment of its suitability for practical applications. There have been many rigorous attempts to quantify the CO_2 capture profile of graphene or its derivatives over a broad range of temperature and pressure conditions (Table 4). These efforts have mostly focused on the measurement of the pure CO_2 gas isotherm: the plot of the amount of gas adsorbed as a function of pressure at a constant temperature.[116] The isotherm is an empirical outcome from which critical information about

11

the quality of the adsorbent material such as adsorption capacity, selectivity and enthalpy of adsorption can be extracted. Although a variety of analytical techniques are available to measure gas adsorption on solids (volumetry, gravimetry, oscillometry, calorimetry, impedance spectroscopy, nuclear resonance and combinations thereof),[117,118] the volumetric (also called manometric) and the gravimetric methods are commonly used to obtain CO_2 isotherms of graphene materials. In the volumetric approach, the volume of a gas adsorbed per unit mass of the adsorbent is determined from the pressure drop before and after adsorption in a closed system using the ideal gas equation.[120] Gravimetric techniques, on the other hand, estimate the quantity of a gas adsorbed by detecting the weight change of the adsorbent sample in response to its exposure to a step change in the gas pressure.[119] While the gravimetric method is inherently more accurate and easier to automate,[120] the volumetric method has been more frequently applied for its simplicity.

One of the primary initiatives to experimentally assess the CO_2 adsorption performance of graphene was reported by Rao and coworkers.[83] They measured the volumetric CO_2 isotherm of graphene samples synthesized from different carbon precursors. At -78 °C and 1 bar, graphene obtained from exfoliation of GO adsorbed up to 7.8 mmol g^{-1} whereas those from thermal conversion of nanodiamonds up to 8.6 mmol g^{-1}. Regardless of the precursor used, CO_2 adsorption on graphene was completely reversible and no significant hysteresis was observed on the desorption branches of the isotherms, suggesting weak intermolecular forces were involved. Moreover, based on DFT calculations the binding energy of a CO_2 molecule was estimated to be -59.1 kJ mol^{-1}, indicating the occurrence of physical adsorption of CO_2 onto graphene. This finding was confirmed by Mishra and Ramaprabhu who examined the uptake of CO_2 by graphene, produced via hydrogen-induced thermal exfoliation of GO at 200 ° C, using infrared (IR) spectroscopy.[84] Beyond the normal hydroxyl (3435 cm^{-1}), carboxyl (1726 cm^{-1}) and carbonyl (1173 cm^{-1}) peaks, a new band corresponding to the asymmetric

stretching of CO_2 appeared at 2324 cm^{-1} in the IR spectra, implying physisorption of CO_2 onto graphene sheets. Mishra and Ramaprabhu further demonstrated that graphene has potential for CO_2 abatement at operating conditions likely to be encountered in an actual industrial flue gas system.[84] They achieved a maximum adsorption capacity of 12 mmol g^{-1} at 11 bar and 100 °C. In another recent work, Wang *et al.* recorded CO_2 and H_2O isotherms for a 3D mesoporous graphene material with a specific surface area of 477 $m^2 g^{-1}$.[85] A major hysteresis appeared between the CO_2 adsorption/desorption isotherms, indicating strong electrostatic interactions between the unsaturated sp^2 bonds at the edge of the graphene plane and the polar CO_2 molecules. No distinct hysteresis loop was observed for H_2O adsorption/desorption isotherms, revealing that the 3D graphene material was highly hydrophobic and hence merits further consideration for capturing CO_2 from wet flue gas.

Graphene as a bulk material, however, has the tendency to form irreversible agglomerates, behaving as particulate graphite platelets, due to strong van der Waals force between the large and planar basal planes. The formation of agglomerates causes a significant decrease of the ultrahigh surface area of 2D graphene sheets.[121] Since gas adsorption behavior is mainly governed by the surface area and pore characteristics of the adsorbent material,[90] the introduction of nanopores into graphene sheets has been identified as one of the most effective methods for improving the adsorption performance of graphene materials.[122] Depending on the pressure at which CO_2 capture will be carried out, pores of different dimension contribute the most: narrow micropores or ultramicropores (pore widths < 0.7 nm) govern the CO_2 uptake at low pressures (i.e., post-combustion applications) whereas at high pressures (i.e., pre-combustion capture) large micropores/small mesopores (pores below 2.0–3.0 nm) are preferred.[123,124] As such, rapid and fruitful developments have been made to introduce nanopores in graphene for better CO_2 adsorption. Owing to their porous structure, such holey graphene scaffolds have a higher surface area and much more "space" for

capturing and storing CO_2 compared to pristine graphene.[121] Meng and Park thermally exfoliated GO sheets in vacuum (Fig. 3, top), producing graphene nanoplates (GNPs) with broad pore size distribution (including supermicropores with widths ~1.2 nm, mesopores between 20−50 nm, and macropores around 90 nm) and appreciable porosity (1.7 $cm^3 g^{-1}$).[86] The GNPs proved to be extremely suitable for separating CO_2 from flue gases at high pressures and room temperature: 56.4 $mmolg^{-1}$ at 25 °C and 30 bar. Meanwhile, Ning *et al*. demonstrated graphene nanomesh (GNM), a novel type of graphene structure with in-plane pores, as excellent candidates for trapping CO_2 at high pressures.[87] The GNM, obtained through CVD using porous layered MgO as template, had a flat box-like structure with specific surface area of up to 2038 $m^2 g^{-1}$ and supermicropores of ~1nm, which resulted in a superior CO_2 uptake of 36.5 $mmolg^{-1}$ at 1°Cand 31 bar. Subsequently, Xia *et al*. synthesized graphene with trimodal micro-meso-macroporous system by CO_2 activation of GO (Fig. 3, bottom).[88] Volumetric gas adsorption experiments indicated that these hierarchical porous graphene (HPG) sheets could adsorb about 1.8 mmol CO_2 per gram at 0 °C and 1 bar. The isosteric heat of adsorption at low surface coverage confirmed physical interactions between CO_2 and HPG. Furthermore, HPG could undergo multiple rounds of recycling without any significant drop in capture efficiency. Likewise, Sui *et. al.* prepared highly efficient graphene-based porous CO_2 adsorbents through steam activation of graphene aerogel.[89] More interestingly, Kumar *et al*. developed porous graphene frameworks (PGFs) via covalent linking of reduced graphene oxide (rGO) layers with 1,4-diethynylbenzene (PGF-1) or 4,4'-diethynylbiphenyl (PGF-2).[90] Due to the C−C coupling between the graphene layers and the linkers, the PGFs displayed large specific surface areas and high thermal stability, as well as good CO_2 storage capacities at both low and high pressures.

There is also a concerted effort to further improve the CO_2 separation ability of graphene for practical deployment. To this end, heteroatom (N, S, B, etc.) doping has been found to endow

graphene materials with greater capacity and selectivity for CO_2.[91-95,125] Kim and colleagues fabricated a series of N- or S-doped graphene-based carbons from different kinds of graphene/polymer composites (graphene/polypyrrole,[91] rGO/polyaniline,[92] rGO/polyindole,[93] and rGO/polythiophene[94]) by chemical (KOH) activation at temperatures in the range of 400−800 °C. The synthesized materials featured high surface area, large pore volume and profound microporosity (Fig. 4). Consequently, the doped graphene samples adsorbed large volumes of CO_2 under ambient conditions (>4 mmol g^{-1}), which was comparable with or even higher than many other solid adsorbents: activated carbons, amine functionalized silica and MOFs. Additionally, the materials had impressive selectivity for CO_2 over N_2 (post-combustion CO_2 capture), H_2 (pre-combustion CO_2 capture), and CH_4 (an important separation for natural gas sweetening) (see Table 4), and could also be easily regenerated for repeated use. A detailed analysis of the adsorption phenomena disclosed that the CO_2 uptake by these high-performance adsorbents was directly correlated to their specific surface area, pore dimensions, as well as the dopant concentration. While high activation temperatures improved the textural characteristics of the samples, it significantly reduced their dopant content. Accordingly, the Kim group recommended that heteroatom-doped graphene procured at relatively lower temperatures (600−700 °C) was suitable for industrial setting. With the same design principle, Oh *et al*. proposed a low-level B-doped graphene adsorbent having excellent recycling property, derived by reacting GO with a borane−tetrahydrofuran (BH_3−THF) adduct, for CO_2 separation processes.[95] The amount of CO_2 adsorbed by B-doped graphene (1.8 mmol g^{-1}) was at least 35% higher than the parent material (1.3 mmol g^{-1}).

Alternatively, non-covalent functionalization with poly (ionic liquid)s (PILs) can also sufficiently enhance the carbon sequestration efficiency of graphene sheets.[96] Upon functionalization, IL moieties uniformly cover graphene, masking the lattice adsorption sites (structural defects). PIL moieties, on the other hand, form porous nanoparticles that are well

distributed on the graphene surface, providing greater access to the adsorption sites. Inevitably, with PIL functionalization a 22% increment in CO_2 adsorption capacity was attained, whereas IL functionalization resulted in just a 2% increase.

Additional attempts to upgrade the CO_2 adsorption properties of graphene have focused on incorporating the bulk material into various organic/inorganic matrices. As depicted in Fig. 5, Zhou *et al*. prepared porous graphene/terpyridine complex hybrids through an azide-alkyne click reaction between alkynl group modified GO (alkynl―GO) and azido-terpyridine complex.[97] The introduction of N-rich terpyridine units between graphene sheets not only increased the surface area and porosity of the materials, but also created more basic sites for adsorbing acidic gases, resulting in a CO_2 capacity of up to 2.7 mmol g^{-1} at 0 ^{o}C and 1 bar. Similarly, Mishra and Ramaprabhu considered graphene/polyaniline composites for CO_2 capture.[98] The composite showed greater CO_2 adsorption than pristine graphene (75 mmol g^{-1} vs. 21.6 mmol g^{-1} at 11 bar and 25 ^{o}C) and also a high degree of recyclability. Fourier transform infrared spectroscopy (FTIR) of the CO_2-loaded composite illustrated that the large volume of gas uptake could be attributed to the chemical interaction of CO_2 with the N-containing functional groups along with molecular adsorption on the surface of the nanostructured graphene/polyaniline hybrid material. Mishra and Ramaprabhu subsequently developed graphene/Fe_3O_4 nanocomposites via *in situ* chemical co-precipitation of Fe^{2+} and Fe^{3+} in alkaline solution in the presence of graphene and investigated its CO_2 adsorption potential at elevated pressures (11 bar).[99] In spite of having a low specific surface area (~98 $m^2 g^{-1}$), graphene/Fe_3O_4 could deliver large CO_2 separation capacities of 60 mmol g^{-1} at 25 ^{o}C which decreased to 24 mmol g^{-1} at 100 ^{o}C. On the basis of FTIR spectral profiles, it was concluded that physicochemical interactions were responsible for the high CO_2 capture by the composite (Fig. 6). In a similar way, Ding and co-workers reported

graphene/Mn_3O_4 porous materials, formulated by a facile hydrothermal reaction, for CO_2 removal at low temperatures and ambient pressure.[100]

Along with binary hybrids, ternary hybrid hierarchical structures have recently been explored as a new strategy to revamp the CO_2 performance of graphene. For example, Yang *et al.* constructed an efficient graphene-based organic-inorganic ternary solid CO_2 adsorbent (PEI/G-silica) using a nanocasting technique outlined in Fig. 7.[101] Such unique architecture enabled a strong synergetic effect of each component: large surface area and high thermal conductivity of graphene (G), uniform porosity and flexible morphology of mesoporous silica, and large CO_2 potential of polyethyleneimine (PEI). As a result, the sandwich-like PEI/G-silica complex boasted an excellent CO_2 capacity (4.3 mmol g^{-1} at 75 ^{o}C) and long-term cycling stability (~20 cycles).

Apart from graphene, its close chemical cousin, graphene oxide (GO), too has received great deal of attention as CO_2 adsorbent. By applying a gas pressurizing technique, Lee and Park produced exfoliated GO that exhibited a strong binding enthalpy (3.5 kJ mol^{-1}) and adsorption capacity for CO_2 (6.4 mmol g^{-1} at 25 ^{o}C) because of its large surface area (547 m^2 g^{-1}) and total pore volume (2.5 cm^3 g^{-1}).[102]Notably, Srinivas *et al.* described the fabrication of highly porous carbon adsorbents, through activation of exfoliated GO precursors with KOH, and their feasibility toward capturing and storing CO_2.[103] From a close comparison with other porous adsorbents including activated carbons and MOFs, it was inferred that the GO derived carbons were truly promising for CO_2 capture applications due to their facile and inexpensive synthesis, tunable porosity, high chemical stability and moderate heat of adsorption. Recently, Sui and Han prepared GO-based 3D hydrogels with interconnected pores by hydrothermal treatment of aqueous GO dispersion at different temperatures (80, 100, and 120 ^{o}C) for 16 h (Fig. 8a-b).[104] While the hydrogel synthesized at 120 ^{o}C showed the

best textural features (specific surface area, 870 m^2 g^{-1}; total pore volume, 2.2 cm^3 g^{-1}), the hydrogel achieved at 100 $^\circ$C registered the highest capacity (2.4 mmol g^{-1} at 0 $^\circ$C and 1 bar) and selectivity for CO_2 (Fig. 8c). Such anomalies in adsorption capacity may be ascribed to strong surface interactions between CO_2 and the hydrogel (involving acid-base interactions, polar interactions, and hydrogen bonding) along with the normal pore-filling process. This was indeed evident from the high isosteric heat of adsorption (51 kJ mol^{-1}) calculated using the classical Clausius-Clapeyron equation.

Impressively, GO is inherently decorated with oxygen-containing functional groups — either on the basal plane or at the edges — allowing it to interact with a wide variety of organic and inorganic materials. There has, therefore, been considerable interest in developing GO-based composites or functional hybrids with enhanced properties for CO_2 adsorption in recent years. For instance, Zhao *et al.* generated a range of amine-functionalized GO materials through an intercalation reaction of GO with alkylamine molecules, including ethylenediamine (EDA), diethylenetriamine (DETA), and triethylenetetramine (TETA), and studied them as solid adsorbents for post-combustion CO_2 capture by performing dynamic adsorption tests with a 15% CO_2 in N_2 gas mixture.[126] As can be seen in Fig. 9, the breakthrough time of the amine-functionalized GO samples decreased in the following order: GO/EDA > GO/DETA > GO/TETA, which was in line with their N-content. The GO intercalated with 50% EDA presented the highest CO_2 capacity (1.1 mmol g^{-1}) under the experimental conditions. Another important contribution that deserves special mention is the development of TiO_2/GO composites for CO_2 adsorption beyond its unambiguous implications in (photo) catalysis.[105] A series of mesoporous TiO_2/GO nanocomposites, with different GO to TiO_2 mass ratios (0.10, 0.20 and 0.30), were synthesized by Chowdhury *et al.* using a simple colloidal blending process and their pure component isotherms were determined up to 1 bar pressure for the temperature range (0 to 50) $^\circ$C. CO_2 adsorption increased with decreasing

temperature and increasing adsorbate concentration. $TiO_2/GO-0.10$ with the lowest GO to TiO_2 mass ratio demonstrated the highest adsorption rate because of its large specific surface area (100 $m^2 g^{-1}$) and total pore volume (0.4 $cm^3 g^{-1}$). The maximum CO_2 adsorption achieved at 25° C and 1 bar was 1.9 mmo lg^{-1}, a value comparatively higher than other solid CO_2 adsorbents including zeolite, activated carbon and some MOFs. Additionally, the rate of adsorption was very fast, and $TiO_2/GO-0.10$ attained saturation levels in just 3 min., $TiO_2/GO-0.10$ also showed a high selectivity in adsorbing CO_2 over N_2 under conditions pertinent to post-combustion applications. Furthermore, the low isosteric heat of adsorption at zero coverage (19.6 $kJ mol^{-1}$) indicated the possibility of desorbing the gas and regenerating the adsorbent at a much lower energy penalty. Based on these findings, it was hypothesized that physisorption as well as chemisorption contributed to the observed composite performance (Fig. 10).

Hydrotalcite-like compounds, an emerging class of materials for removing a range of acidic molecules (e.g., H_2S, SO_X, HCl and CO_2) from many industrial processes and waste streams,[19] have also been composited with GO for effective CO_2 capture from flue gas. Garcia-Gallastegui and colleagues directly precipitated Mg—Al layered double hydroxide(s) (LDH) onto GO sheets in a "layer-by-layer" fashion, followed by calcination at 400 °C in N_2 atmosphere for 4 h, to obtain GO/LDH heterostructured nanohybrids.[106] High temperature CO_2 adsorption measurements revealed that both CO_2 uptake and multicycle stability of the GO/LDH composite was considerably higher than that of the pure LDH (Fig. 11). In a near identical study, Iruretagoyena et al. investigated layered double oxide(s) (LDO) supported on GO sheets for CO_2 sequestration.[107] Multicycle temperature swing and isothermal N_2 purge experiments suggested that the GO/LDO composites retained a greater CO_2 capacity and stability compared to pure LDO or pristine GO. Most importantly, the presence of moisture

had a positive influence on CO_2 removal due to formation of new adsorption sites as a result of surface rehydration of GO/LDO.

Cross-linking GO with polymers can further lead to high-performing CO_2 adsorbents. Sui *et al*. devised a facile approach to the preparation of lightweight GO/PEI porous materials with 3D interconnected networks under mild conditions (Fig. 12).[108] The GO/PEI with bulk densities in the range of 0.02−0.03 $g\,cm^{-3}$ displayed a large specific surface area (476 $m^2\,g^{-1}$) and total pore volume (1.3 $cm^3\,g^{-1}$), offering enormous technological promise for CO_2 emission reductions. Alhwaige and co-workers almost simultaneously reported GO/chitosan hybrid aerogels as exciting new adsorbents for CO_2 capture.[109] N_2 (−196 °C) adsorption/desorption measurements corroborated that increasing GO content dramatically increased the specific surface of the GO/chitosan aerogels (Fig. 13). Consequently, the aerogel with the highest GO loading (20%) gave the maximum CO_2 uptakeat ambient temperature and atmospheric pressure (Fig. 13). In addition, the GO/chitosan aerogels showed easy regeneration and good stability over multiple cycles, which is extremely beneficial from a practical viewpoint.

Most recently, Tsoufis *et al*. intercalated low molecular weight DAB (diaminobutane poly-propylene-imine) dendrimers into the interlayer spacing of GO sheets without the use of any cross-linking agent and evaluated the CO_2 adsorption potential of the resulting GO/DAB hybrids under conditions relevant to post-combustion capture.[110] Gravimetric gas adsorption measurements indicated that GO/DAB had greater adsorption ability and faster kinetics under wet conditions than under dry conditions. The improvement in adsorption upon wetting could be due to reaction of CO_2 with the primary (through the formation of a zwitterion as an intermediate) and tertiary (by base-catalyzed hydration) amines of the DAB dendrimer to form carbamates and bicarbonates, respectively. Additionally, the presence of water

molecules on GO/DAB favored the formation of continuous liquid phase channels, which in turn increased the solubility of CO_2 in the water phase, thereby augmenting the adsorption kinetics. It therefore appears that investigating the effect of water vapor on the CO_2 adsorption properties of graphene material is of utmost importance. The CO_2 uptake profile, as determined from pure-component isotherms, may not always be the best indicator of adsorbent performance in a real-world CO_2 capture process and hence the need for addressing the effects of water vapor.

Other than inorganic nanostructures and polymers, MOFs have also been recently composited with GO for the synthesis of novel adsorbents with unique characteristics to efficiently capture CO_2 from existing emission sources. In a seminal report, Rao and co-workers described the preparation of GO/ZIF-8 hybrid nanocomposites as intriguing candidates for high volume CO_2 capture (Fig. 14a).[111] By fine-tuning the GO content, the surface area, pore volume as well as the nanoscale morphology of the composite (from hexagonal to spherical) could be rationally controlled (Fig. 14b). The CO_2 capacity of the GO/ZIF-8 composites was remarkably higher compared to the parent MOF and increased with increasing GO concentration. This was attributed to the synergistic effect of ZIF-8 and GO, where the latter provided additional interaction sites for CO_2. Furthermore, in a subsequent publication, the Rao group demonstrated GO/Cd-PBM[a] composites for highly selective adsorption of CO_2 from N_2.[127] Simultaneously, inspired by the findings of the Rao group, Huang *et al*. synthesized GO/Cu-BTC composites using a solvothermal method for the separation of CO_2/CH_4 binary mixture.[112] The adsorption of CO_2 by GO/Cu-BTC (8.2 mmol g^{-1} at 0 °C and 1 bar) was higher than that of pristine Cu-BTC (6.5 mmol g^{-1} at 0 °C and 1 bar), estimated from single-component gas adsorption isotherms. Analysis of the CO_2/CH_4

---

[a] $\{[Cd_4(azpy)_2(pyrdc)_4(H_2O)_2]\cdot 9H_2O\}_n$ (azpy = 4,4'-azopyridine, pyrdc = pyridine-2,3-dicarboxylate)

adsorption selectivity on the basis of ideal adsorbed solution theory (IAST) further established the efficacy of the GO/Cu-BTC composite (14 at 1 bar or 2.6 times that of Cu-BTC) in CO_2 removal applications (Fig. 15). Another significant contribution recently came from Zhou *et al*. who showed that the introduction of a small fraction of GO to MIL-101 framework can result in a robust GO/MIL-101 composite adsorbent with enhanced porosity and improved CO_2 uptake.[113] The CO_2 capacity of GO/MIL-101 at 25 °C and 25 bar was much higher than many traditional adsorbents and most other MOFs including MIL-101. Moreover, IAST calculations revealed that CO_2 was more favorably adsorbed than CH_4 on GO/MIL-101. In addition, GO/MIL-101 displayed a readily reversible adsorption/desorption under PSA conditions. In a similar manner, Cao and colleagues tested GO/UiO-66 as CO_2 adsorbents at room temperature.[114] The composite exhibited higher surface area and micropore volume compared to UiO-66 (1184 m^2 g^{-1} and 0.3 cm^3 g^{-1} vs. 838 m^2 g^{-1} and 0.2 cm^3 g^{-1}), whereby as much as 3.4 mmol g^{-1} CO_2 could be adsorbed at 25 °C and 1 bar. Moreover, the GO/UiO-66 manifested a stable adsorption/desorption cycling behavior for continuous operation. Very recently, Bian *et al.* developed a facile IL-assisted method for *in situ* growth of $Cu_3(BTC)_2$ MOF on GO sheets for improved CO_2 adsorption (Fig. 16).[115] Three different ILs, namely triethylenetetramine acetate (TETA-Ac), triethylenetetraminetetrafluoroborate (TETA-BF4) and 1-Butyl-3-methylimidazolium tetrafluoroborate([Bmim]BF$_4$), were used to investigate the effect of their chemical make-up on the structure and morphology of the resulting ternary composites. Due to its four amine groups in the cation and the contrary acetate anion, TETA-Ac produced GO-IL/MOF composite with the largest surface area (2043 m^2 g^{-1}) and total pore volume (0.2 cm^3 g^{-1}). As a result, GO-TETA-Ac/$Cu_3(BTC)_2$ showed a high CO_2 adsorption capacity of 5.6 mmol g^{-1} and a high CO_2/N_2 selectivity of 21 at 25 °C and 1 bar. Above all, the composite presented a high CO_2 kinetic separation as well as good cyclic adsorption/desorption stability.

22

4.2. Computational simulations and predictions

With recent growth in computational power, molecular simulations can now provide valuable insights into the interaction of adsorbate molecules with the adsorbent surface, enhancing our ability to interpret experimental observations based on an adsorbent's atomic scale properties and macroscopic functionality.[128] Such in-depth fundamental information on an adsorbent's molecular structure in conjunction with experimental data is particularly important for the rational design of new adsorbents tailored to meet the intended operating conditions. In addition, molecular simulations constitute an extremely powerful tool for rapid and systematic screening of both existing and hypothetical adsorbents, necessitating experimental validation of only those that demonstrate the highest level of performance, thus saving time and resources.[129] In view of these explicit benefits, there is a growing interest in applying molecular simulation techniques to assess and predict CO_2 adsorption on graphene-based materials (Table 5). Much of this work has been shaped and fueled by the general availability of quality simulation facilities including quantum calculations (i.e., density functional theory (DFT) and *ab initio* simulations), Grand Canonical Monte Carlo (GCMC) simulations, and molecular dynamics (MD) simulations.

The first molecular simulation of CO_2 adsorption on graphene was reported by Cabrera-Sanfelix,[130] who carried out DFT calculations to explore the adsorption of CO_2 on defective graphene sheets (with single vacancy) because of their higher chemical reactivity for small molecules compared with pristine (defect-free) graphene (Fig. 17a-c). CO_2 was indeed strongly physisorbed on top of the vacancy defect with physisorption energy of $\sim$13.1 kJ mol^{-1} (Fig. 17d). The molecule was then subsequently chemisorbed at the vacancy defect of the graphene layer, after overcoming an energy barrier of about 96.5 kJ mol^{-1} relative to the gas phase, by forming a "lactone complex" with an exothermicity of 135.1 kJ mol^{-1} (Fig. 17e). Following this pioneering study, Liu and Wilcox applied the plane-wave electronic

DFT calculations to develop a more rigorous understanding of the underlying mechanism of CO_2 adsorption on defective graphene surfaces.[131] Specifically, the interaction of CO_2 with graphene surfaces containing (i) a monovacancy, (ii) a pentagon–octagon–pentagon (5–8–5) double vacancy, and (iii) the Stone-Wales defect was investigated. The results of DFT optimization implied that CO_2 binding affinity of defective graphene was relatively higher than its pristine counterpart. The physisorption energy of CO_2 on the defective graphene site with one carbon atom missing (i.e. monovacancy) was four times as strong as that on a perfect defect-free graphene surface (20.3 kJ mol^{-1} on the monovacancy site compared to 4.8 kJ mol^{-1} on pristine graphene). Based on these findings, one may envisage that the controlled introduction of vacancy defects is a possible scheme to drastically improve the CO_2 adsorption profile of graphene.

Ohba and Kanoh inspected the variation in the interaction potentials of edge sites and basal planes of nanographene for CO_2 and N_2 using GCMC simulations.[132] They found that CO_2 preferred to be adsorbed on the edge sites whereas N_2 on the basal planes. Accordingly, it was reasoned that edge sites of nanographene were centers of strong Columbic interaction because of partial charges at the edges, but basal planes had no partial electronic charges, corresponding to near-zero Columbic interaction. As a result, CO_2 with appreciably higher quadrupole moment than N_2 was preferentially adsorbed to the edge sites in the low-pressure region. To our knowledge, this work is the first and perhaps the only simulation-based account on edge effects of nanographene on CO_2 adsorption. The results provide preliminary evidence to build adsorbents for selective separation of CO_2 from post-combustion flue gas mixture via precise tuning of graphene edges.

In gas adsorption processes, separation is based on differences in the physical properties of the gases, such as polarizability and quadrupole moment, which results in a higher enthalpy

of adsorption for certain molecules over others. As can be seen from Table 2, CO_2 is a highly

quadrupolar gas while the other gases which are likely to be encountered in a CO_2 capture

system, including N_2, O_2 and H_2, are non-polar or weakly polar. It is therefore intuitively

appealing to improve the adsorption capacity and selectivity of graphene by the introduction

of functional groups having high affinity for CO_2. A good example in this context is the work

of Wood et al.[133] Using DFT simulations, they systematically quantified the effect of grafting

diverse functional substituents ($-OH$, $-NH_2$, $-CH_3$, $-NO_2$, $-COOH$, and $-H_2PO_3$) on the

interaction of CO_2 with zigzag graphene nanoribbons. In fact, polar groups, including $-$

COOH, $-NH_2$, $-NO_2$, and $-H_2PO_3$, proved promising for enhancing CO_2 adsorption by

activating exposed edges and terraces to act as suitable gas binding sites. In another recent

study, Dasgupta et al. investigated the influence of specific functional moieties on the

selective separation of CO_2 from CO_2/N_2 mixtures using a combination of ab initio and

classical Monte Carlo simulations.[134] A bilayer graphene nanoribbon, edge functionalized

with $-OH$, $-NH_2$, $-NO_2$, $-CH_3$, and $-COOH$ groups, was considered for this purpose. The

results of ab initio calculations carried out by employing the second-order Møller-

Plesset perturbation theory (MP2) method confirmed that functionalization augments CO_2 as

well as N_2binding with the greatest enhancement shown by $-COOH$ (Fig. 18a), which could

be attributed to the overall increase in van der Waals interactions owing to the presence of

C=O bond. Equilibrium adsorption capacities and heats of adsorption obtained at a

temperature of 25 ^{o}C and pressures up to 20 bar using GCMC simulations further ascertained

that the $-COOH$ group instituted the maximum increment for both CO_2 and N_2.

Nevertheless, the surface excess and heats of adsorption for CO_2 were remarkably higher than

those for N_2 across the functional groups investigated (Fig. 18b). Besides, the $-COOH$

functionalization resulted in a notable improvement in the selectivity for CO_2 over N_2 (by

almost 28%). From these studies, it can be concluded that site specific functionalization with

–COOH has a prominent effect on the local gas adsorption characteristics and may be explored as a potential route to manipulate graphene sheets for high CO_2 capacity and selectivity.

Computational efforts have further demonstrated that doping graphene with metal ions can also improve its efficiency of capturing CO_2. Carrillo *et al*. examined the uptake of CO_2 by a graphene layer with high titanium coverage at atmospheric pressure and 27 $^{\circ}$C (see Fig. 19a), using DFT and molecular dynamics simulation.[135] On the basis of their calculations, Carrillo *et al*. proposed a plausible mechanism of CO_2 adsorption in titanium–graphene (C_2Ti) system. The CO_2 molecule is linear, positively charged at the C atom and negatively charged at the O atoms. When it is brought near the C_2Ti surface, the positively charged Ti atoms exert a strong attraction for the negatively charged O atoms. Obviously, this electrostatic force is stronger than the repulsion force on the C atom by the Ti atoms. As the CO_2 molecule gradually move closer toward C_2Ti, the O atoms being under different force fields bend the CO_2 molecule. One of the O atoms traps electronic charges from the Ti atoms of the upper plane and ends up bonding to four Ti atoms, thereby dissociating CO_2 into CO and O. The CO fraction is then adsorbed on the C_2Ti surface in a manner that the C atom is bonded to three Ti atoms while the O atom is bonded to another Ti atom, as illustrated in Fig. 19b. It is therefore likely that inclusion of monodispersed Ti atoms onto graphene surface will significantly increase its CO_2 capture performance. Likewise, Cazorla *et al*.[136] conducted a systematic simulation-based research to assess the CCS potential of Ca-doped graphene. CO_2 molecules were observed to bind very weakly to pristine graphene and preferred to accommodate on top of subjacent C–C bonds (Fig. 20a). In contrast, the interaction of CO_2 with Ca-doped graphene was relatively strong and the strength of the binding could be efficiently tuned by altering the metal dopant concentration. Intense molecular binding accompanied by large electronic charge transfers was noticed at low dopant concentrations

(Fig. 20b) whereas in case of high dopant concentrations, CO_2 molecules were physisorbed

on the graphene surface (Fig. 20c). This implies that densely doped graphene would be ideal

for low-temperature/low-pressure CCS application (e.g., post-combustion capture) whereas

sparsely doped graphene would be promising for high-temperature/high-pressure CCS

practice (e.g., pre-combustion capture). The CO_2/N_2 adsorption selectivity was also inspected

with the finding that N_2 binds to Ca-doped surface more weakly than CO_2. Thus, Ca-doped

graphene may be potentially applicable to carbon capture processes. By using first-principles

calculations, doping of GO with light metals (Li, Al) has also been recently proposed as an

attractive approach for highly efficient CO_2 capture from flue gas streams.[137]

Another useful strategy for improving the CO_2 uptake potential of graphene is the

incorporation of other carbon-based materials, such as fullerenes, into graphene sheets. Using

GCMC simulations, Terzyk *et al*. showed that CO_2 adsorption capacity of fullerene

intercalated graphene nano-containers was amplified by increasing fullerene concentration of

the composite system.[138] Terzyk *et al.* also observed that pores with effective diameter of ca.

0.5 nm were competent for CO_2 removal at low pressures due to energetically favorable

surface interactions. Conversely, larger slit pores (diameters in the range 1–2.4 nm) were

found appropriate for CO_2 capture under high pressure conditions owing to multilayer

molecular adsorption.

Recently, the modification of GO layers through intercalation has been studied as a powerful

alternative to develop new adsorbents with tailored properties for CO_2 capture applications.

For example, Garberoglio *et al*. theoretically created a three-dimensional (3D) GO

framework (GOF) pillared by organic linkers using DFT based atomistic simulations as

shown in Fig. 21.[139] GCMC simulations were then implemented at –78 °C for gas pressures

up to 1 bar to predict the CO_2 adsorption properties of the developed framework. Their

simulation results suggested that the rate of CO_2 uptake was a function of the density of pillars and the specific chemical moiety used as spacer. Moreover, the constructed 3D framework also displayed a high CO_2/H_2 selectivity at 25 $^{\circ}$C and pressures below ~0.5 bar. Garberoglio *et al*. attributed this observation to the thermodynamically favorable interaction of CO_2 with GOF at low pressures.

It is well acknowledged that the considerable volume of combustion water in flue gas is a serious impediment to adsorption-based CO_2 capture. Water can have negative impacts on an adsorbent's CO_2 selectivity and also on capacity, owing to its competition with CO_2 for the adsorption sites. Computational attempts focusing on the influence of water on the CO_2adsorption strength of graphene materials have therefore also begun to emerge. Yumura and Yamasaki employed DFT calculations to understand the role of water molecules in trapping CO_2 inside the interlayer space of GO.[140] A detailed analysis of the simulation data revealed that CO_2 interacts repulsively with anhydrous GO layers to increase the interlayer spacing, which is reduced in the presence of water molecules because of the occurrence of attractive water–layer interactions through hydrogen bonding. The DFT calculations further indicated that the GO interlayer spacing, which is affected by the intercalation of water molecules, controls CO_2 migration within the GO layers. When the GO interlayer distance is less due to the existence of intercalated water molecules, the fairly strong repulsive interactions between CO_2 and GO avert the migration of CO_2 from its original binding position. Such repulsive interactions do not arise during the migration of CO_2 within anhydrous GO structures owing to the relatively longer interlayer distance. Accordingly, migration of CO_2 within anhydrous GO involves much lower energy barriers, implying that CO_2 molecules are easily released from the GO layers. These findings are undoubtedly useful for the development of next-generation graphene-based adsorbents exhibiting improved moisture resistance for post-combustion capture.

Overall, there has been a significant amount of research resorting to different molecular simulation tools for elucidating the CO_2 adsorption properties of graphene-based materials. In addition to providing quantitative information (such as CO_2 uptake capacity, CO_2/N_2 selectivity, and heat of adsorption), computer simulations also present the unique opportunity to deduce the underlying CO_2 uptake mechanism, which would otherwise require expensive and tedious experimental settings. Considering the vast array of possibilities available for engineering new graphene-based adsorbents, it would be both judicious and thoughtful to systematically screen graphene-based systems using molecular simulation methods in order to identify the most ideal candidates for CO_2 capture applications. However, the combination of computational research with laboratory experiments is imperative to successfully realize the true potential of such promising graphene-based structures for reducing CO_2 emissions from fossil fuel-fired power plants.

5. Outlook and future perspectives

Clearly, a broad range of graphene materials have been investigated, both theoretically and experimentally, to curb CO_2 emissions from static sources of fossil fuel combustion. Based on the critical analysis of all findings discussed above, a consensus emerges that graphene and its derivatives possess the ability to capture CO_2, specifically in terms of high storage, excellent selectivity, rapid uptake, easy regeneration, and good reproducibility and stability. Many of the graphene-based materials exhibit CO_2 adsorption capacities comparable to or exceeding those of the best activated carbons, zeolites and MOFs. However, a number of technological limitations and practical challenges have to be tackled in order to produce next-generation graphene-based adsorbents with the capability of being applied on an industrial scale for efficient and effective CO_2 separation from flue gases. To achieve this desired outcome, the following recommendations are made for further research (Fig. 22):

(i) *Measurement of CO_2 uptake on volumetric basis*

The adsorption capacity is undoubtedly one of the most critical parameters when evaluating a new material for CO_2 capture applications. While the gravimetric capacity (i.e., the mass of gas adsorbed per unit mass of adsorbent) estimates the amount of an adsorbent required to be packed in a continuously operating adsorption system, the volumetric capacity (i.e., the volume of gas adsorbed under standard conditions divided by the volume of adsorbent) has a significant impact on the volume of the adsorbent bed and hence the size of the CO_2 recovery apparatus.[141] Consequently, the volumetric uptake appears to be the most appropriate metric to quantify the CO_2 adsorption capacity of any adsorbent. However, based on the literature reviewed, CO_2 adsorption in graphene materials has been found to be commonly measured on a gravimetric basis with no data on volumetric uptake currently available. Therefore, the volumetric CO_2 adsorption capacity should be determined and provided as part of laboratory-based investigations, which in turn would enable the prospects of applying these nanomaterials in an industrial setting to be more accurately evaluated.

(ii) *Evaluation of working capacity*

Another important metric for evaluating any adsorbent is the CO_2 working capacity, determined by measuring the difference between the amounts of a gas adsorbed at adsorption and desorption pressures. From a practical viewpoint, a good working capacity is highly desirable since the quantity of an adsorbent needed to construct the adsorption column can be reduced considerably.[30] This in turn lowers the initial capital costs as well as leads to long-term energy benefits for regeneration.[30] Future research work in graphene-based CO_2 adsorbents should also focus on calculating the maximum working capacity in order to ascertain their large scale deployment.

(iii) *Measurement of multicomponent gas adsorption isotherms*

Most of the adsorption experiments have been carried out with a single component system i.e., CO_2 only with no other gases in the matrix that can potentially compete for the limited number of adsorption sites on the adsorbent. While single component isotherms provide precise information on the CO_2 uptake capacity of an adsorbent, multicomponent isotherms are of greater importance for assessing the performance of an adsorbent under conditions expected to be encountered in an actual CO_2 capture system.[142] For example, with reactive gases (SO_2, NO_X, and CO) present in an industrial flue gas, complex interactions between CO_2 and various flue gas constituents can occur at the adsorbent surface which can in turn affect its capture efficiency. To our knowledge, no direct measurements of such multicomponent isotherms in graphene materials are currently available in the literature. Even though some researchers have attempted to predict the multicomponent equilibrium from pure component isotherms (using IAST), such predictions are, however, not accurate enough for process development because of their intrinsic limitations.[143] Future research must therefore address this issue if graphene or its derivatives are to be employed in a real-world CO_2 capture system.

(iv) *Determination of the influence of water vapor*

When evaluating graphene-based materials for applications in a CO_2 capture process, it is further important to consider the effect of moisture on the separation of CO_2 since the flue gas usually contains significant volumes of water vapor which can in turn affect the adsorption process. While some attempts have been made to record the CO_2 adsorption profile of graphene materials under humid conditions, most existing studies do not rigorously evaluate the performance of these materials upon repeated exposure to moisture. A better understanding of the influence of water vapor on carbon capture is therefore urgently needed,

which would eventually assist in the rational design of more advanced graphene-based CO_2 adsorbents that are water-repellent.

(v) *In situ characterization of adsorbed CO_2*

In situ characterization methods are of great importance for studying the relationship between the structural and chemical features of an adsorbent and its observed adsorption performance.[144] Future research should therefore focus on crystallographic characterization of CO_2-loaded graphene materials with *in-situ* analytical techniques such as XRD, IR or NMR spectroscopy for direct observations of the location of CO_2 molecules within the molecular structure of the adsorbents.[b] The outcome of this work would facilitate a fundamental understanding of the gas adsorption mechanism and thus contribute toward designing more advanced graphene-based CO_2 adsorbents.

(vi) *Development of molecular models and force fields mimicking realistic conditions*

In parallel with experimental studies, molecular simulation methods must be further developed as a tool to predict the performance of graphene materials for CO_2 separation. Currently, much of the simulation-based work has been performed under highly idealized conditions, and less attention has typically been given to provide deep understanding of the CO_2 uptake performance of graphene materials when exposed to operating environment similar to those encountered in industrial settings. Hence, developing molecular models and force fields based on actual flue gas conditions is a prerequisite for the successful screening and evaluation of new graphene-based CO_2 adsorbents.

Beyond these considerations, the engineering economics of graphene materials must be evaluated upon scaling-up the materials for industrial applications, and economic models

---

[b] X-ray diffractometry (XRD), Nuclear magnetic resonance spectroscopy (NMR)

must be established to perform life cycle assessment in order to ascertain the feasibility of bulk preparations of the most promising graphene-based adsorbents.

6. Conclusion

The development of new adsorbents with high capacity and high selectivity for reducing energy-related CO_2 emissions is a topic of utmost global importance because of its implications in climate change mitigation. Recent advances in materials science and engineering suggest that graphene, a wonder material with many attractive properties, can deliver viable solutions to the challenges of developing cost-effective, energy efficient and high-volume adsorption-based CO_2 capture technologies. This review therefore integrated the recent research progress in the development of graphene and its derivatives as next-generation of CO_2 adsorbents. Indeed it is apparent from the existing literature that graphene's unique structure and highly interesting properties provide vast opportunities for designing and fabricating robust adsorbents that are truly well-suited to be deployed in an industrial setting. Both experimentation and molecular simulation studies demonstrate the immense potential of graphene-based materials for capturing and isolating CO_2 from fossil fuel combustion-derived flue gas streams. In comparison to other competing adsorbents, a key advantage of these 2D material systems is that many different functional groups or heteroatoms can be attached to their surface, allowing custom-tailoring of surface properties without sacrificing the remarkable intrinsic characteristics of the graphene core. Nonetheless, this field of investigation is still at its early development stage. There are many research gaps and technical challenges that need immediate attention if the outcome of laboratory-based investigations on these promising nanostructures is to be translated into real-world CO_2capture applications. This inevitably calls for a broad interdisciplinary and integrated

research initiative, which would in turn ultimately lead to a low-carbon future by reducing CO_2 emissions from coal-burning power plants and other stationary sources.

Acknowledgements

Notes and references

1. D. Toporov, *Combustion of Pulverised Coal in a Mixture of Oxygen and Recycled Flue Gas*, Elsevier Ltd., London (UK), 2014.

2. P.J. Reddy, *Clean Coal Technologies for Power Generation*, CRC Press, Florida (USA), 2013.

3. IEA, *Energy Technology Perspectives 2010: Scenarios and Strategies to 2050*, OECD Publishing, Paris (FR), 2009.

4. D.P. Schrag, *Science*, 2007,**315**, 812-813.

5. S. Chu and A. Majumdar, *Nature*, 2012,**488**, 294-303.

6. IEA, *Energy Technology Perspectives 2012: Pathways to a Clean Energy System*, OECD Publishing, Paris (FR), 2012.

7. IPCC, *Climate Change 2014: Mitigation of Climate Change. Contribution of Working Group III to the Fifth Assessment Report of the Intergovernmental Panel on Climate Change*, Cambridge University Press, Cambridge (UK), 2014.

8. R.S. Haszeldine, *Science*, 2009,**325**, 1647–1652.

9. Q. Wang, J. Luo, Z. Zhong and A. Borgna, *Energy Environ. Sci.,* 2011, **4**, 42-55.

10. M. Olivares-Marin and M.M. Maroto-Valer, *Greenhouse Gas. Sci. Technol*., 2012, **2**, 20-35.

11.   A.T. Najafabadi, *Renew. Sust. Energ. Rev.*, 2015, **41**, 1515-1545.

12.   A.A. Olajire, *Energy*, 2010, **35**, 2610-2628.

13.   M.K. Mondal, H.K. Balsora and P. Varshney, *Energy*, 2012, **46**, 431-441.

14.   S.D. Kenarsari, D. Yang, G. Jiang, S. Zhang, J. Wang, A.G. Russell, Q. Wei andM. Fan, *RSC Adv.*, 2013,**3**, 22739–22773.

15.   I. Hadjipaschalis, G. Kourtis and A. Poullikkas, *Renew. Sust. Energ. Rev.*, 2009, **13**, 2637-2644.

16.   V. Scott, S. Gilfillan, N. Markusson, H. Chalmers and R.S. Haszeldine, *Nat. Clim. Change*, 2013, **3**, 105-111.

17.   M. Pera-Titus, *Chem. Rev.*, 2014, **114**, 1413-1492.

18.   J. Wilcox, R. Haghpanah, E.C. Rupp, J. He and K. Lee, *Annu. Rev. Chem. Biomol. Eng.*, 2014, **5**, 479-505.

19.   L.K.G. Bhatta, S. Subramanyam, M.D. Chengala, S. Olivera and K. Venkatesh, *J. Clean. Prod.*, 2015, **103**, 171-196.

20.   T.C. Drage, C.E. Snape, L.A. Stevens, J. Wood, J. Wang, A.I. Cooper, R. Dawson and X. Guao, in *Proceedings of the 3rd International Gas Processing Symposium: Qatar, March 2012*, ed. A. Aroussi and F. Benyahia, Elsevier Ltd., Oxford (UK), 2012, pp. 30-37.

21.   J.-R. Li, R.J. Kuppler and H.-C. Zhou, *Chem. Soc. Rev.*, 2009, **38**, 1477-1504.

22.   C.A. Scholes, K.H. Smith, S.E. Kentish and G.W. Stevens, *Int. J. Greenh. Gas. Con.*, 2010, **4**, 739-755.

23.   K. Goto, K. Yogo and T. Higashii, *Appl. Energy*, 2013, **111**, 710-720.

24.   C. Lastoskie, *Science*, 2010, **330**, 595-596.

25.   Z.H. Lee, K.T. Lee, S. Bhatia and A.R. Mohamed, *Renew. Sust. Energ. Rev.*,2012, **16**, 2599-2609.

26.   S. Choi, J.H. Drese and C.W. Jones, *ChemSusChem*, 2009, **2**, 796-854.

27.   R. Sabouni, H. Kazemian and S. Rohani, *Environ. Sci. Pollut. Res.*, 2014, **21**, 5427-5449.

28.   A.S. Bhown and B.C. Freeman, *Environ. Sci. Technol.*, 2011, **45**, 8624–8632.

29.   Y.-S. Bae and R.Q. Snurr, *Angew. Chem. Int. Ed.*, 2011, **50**, 11586-11596.

30.   K. Sumida, D.L. Rogow, J.A. Mason, T.M. McDonald, E.D. Bloch, Z.R. Herm, T.-H. Bae and J.R. Long, *Chem. Rev.*, 2012, **112**, 724-781.

31.   S. Rackley, *Carbon Capture and Storage*, Butterworth-Heinemann, Oxford (UK), 2009.

32. A. Sayari, Y. Belmabkhout and R. Serna-Guerrero, *Chem. Eng. J.*, 2011, **171**, 760-711.

33. Y. Liu, Z.U. Wang and H.-C. Zhou, *Greenhouse Gas. Sci. Technol.*, 2012, **2**, 239-259.

34. A. Samanta, A. Zhao, G.K.H. Shimizu, P. Sarkar and R. Gupta, *Ind. Eng. Chem. Res.*, 2012, **51**, 1438-1463.

35. B.P. Spigarelli and S.K. Kawatra, *J. CO_2 Util.*, 2013, **1**, 69-87.

36. O. Cheung and N. Hedin, *RSC. Adv.*, 2014, **4**, 14480-14494.

37. A.-H. Lu and G.-P. Hao, *Annu. Rep. Prog. Chem., Sect. A: Inorg. Chem.*, 2013, **109**, 484-503.

38. J. Wang, L. Huang, R. Yang, Z. Zhang, J. Wu, Y. Gao, Q. Wang, D. O'Hare and Z. Zhong, *Energy Environ. Sci.*, 2014, **7**, 3478-3518.

39. S.-Y. Lee and S.-J. Park, *J. Ind. Eng. Chem.*, 2015, **23**, 1-11.

40. R. Thiruvenkatachari, S. Su, H. An and X.X. Yu, *Prog. Energ. Combust.*, 2009, **35**, 438-455.

41. S. Keskin, T.M. van Heest and D.S. Sholl, *ChemSusChem*, 2010, **3**, 879-891.

42. J. Liu, P.K. Thallapally, B.P. McGrail, D.R. Brown and J. Liu, *Chem. Soc. Rev.*, 2012, **41**, 2308-2322.

43. S. Jana, S. Das, C. Ghosh, A. Maity and M. Pradhan, *Sci. Rep.*, 2015, doi:10.1038/srep08711.

44. A.K. Geim and K.S. Novoselov, *Nat. Mater.*, 2007, **6**, 183-191.

45. V. Singh, D. Joung, L. Zhai, S. Das, S.I. Khondaker and S. Seal, *Prog. Mater. Sci.*, 2011, **56**, 1178-1271.

46. K.S. Novosleov, V.I. Fal'ko, L. Colombo, P.R. Gellert, M.G. Schwab and K. Kim, *Nature*, 2012, **490**, 192-200.

47. Y.B. Tan and J.-M. Lee, *J. Mater. Chem. A*, 2013, **1**, 14814-14843.

48. Y. Shao, M.F. El-Kady, L.J. Wang, Q. Zhang, Y. Li, H. Wang, M.F. Mousavi and R.B. Kaner, *Chem. Soc. Rev.*, 2015, **44**, 3639-3665.

49. J. Hou, Y. Shao, M.W. Ellis, R.B. Moore and B. Yi, *Phy. Chem. Chem. Phys.*, 2011, **13**, 15384-15402.

50. C. Xu, B. Xu, Y. Gu, Z. Xiong, J. Sun and X.S. Zhao, *Energy Environ. Sci.*, 2013, **6**, 1388-1414.

51. R. Raccichini, A. Varzi, S. Passerini and B. Scrosati, *Nat. Mater.*, 2015, **14**, 271-279.

52. B.F. Machado and P. Serp, *Catal. Sci. Technol.*, 2012, **2**, 54-75.

53. S. Chowdhury and R. Balasubramanian, *Appl. Catal., B*, 2014, **160-161**, 307-324.

54. D. Chen, H. Zhang, Y. Liu and J. Li, *Energy Environ. Sci.*, 2013, **6,** 1362-1387.

55.   J. Liu, Z. Liu, C.J. Barrow and W. Yang, *Anal. Chim. Acta.*, 2015, **859**, 1-19.

56.   X. Wang, W. Xie and J.-B. Xu, *Adv. Mater.*, 2014, **26**, 5496-5503.

57.   B. Garg, C.-H. Sung and Y.-C. Ling, *Wiley Interdiscip. Rev. Nanomed. Nanobiotechnol.*, 2015, doi: 10.1002/wnan.1342.

58.   C. Zhu, T. Yong-Jin Han, E.B. Duoss, A.M. Golobic, J.D. Kuntz, C.M. Spadacciniand M.A. Worsley, *Nat. Commun.*, 2015, doi: 10.1038/ncomms7962.

59.   S. Goenka, V. Sant and S. Sant, *J. Control. Release*, 2014, **173**, 75-88.

60.   J. Liu, L. Cui and D. Losic, *ActaBiomater.*, 2013, **9**, 9243-9257.

61.   A. Aghigh, V. Alizadeh, H.Y. Wong, M.S. Islam, N. Amin and M. Zaman, *Desalination*, 2015, **365**, 389-397.

62.   P.S. Goh and A.F. Ismail, *Desalination*, 2015, **365**, 115-128.

63.   S. Gadipelli and Z.X. Guo, *Prog. Mater. Sci.*, 2015, **69**, 1-60.

64.   G. Liu, W. Jin and N. Xu, *Chem. Soc. Rev.*, 2015, **44**, 5016-5030.

65.   J. Chang, G. Zhou, E.R. Christensen, R. Heideman and J. Chen, *Anal. Bioanal. Chem.*, 2014, **406**, 3957-3975.

66.   Y. Shen, Q. Fang and B. Chen, *Environ. Sci.Technol.*, 2015, **49**, 67-84.

67.   H. Wang, X. Yuan, H. Huang, X. Peng, G. Zeng, H. Zhong, J. Liang and M. Ren, *Adv. Colloid. Interface Sci.*, 2013, **195-196**, 19-40.

68.   K.C. Kemp, H. Seema, M. Saleh, N.H. Le, K. Mahesh, V. Chandra and K.S. Kim, *Nanoscale*, 2013, **5**, 3149-3171.

69.   S. Chowdhury and R. Balasubramanian, *Adv. Colloid. Interface Sci.*, 2014, **204**, 35-56.

70.   F. Perreault, A.F. de Faria and M. Elimelech, *Chem. Soc. Rev.*, 2015, **44**, 5861-5896.

71.   J.-G. Yu, L.-Y. Yu, H. Yang, Q. Liu, X.-H. Chen, X.-Y. Jiang, X.-Q. Chen and F.-P. Jiao, *Sci. Total Environ.*, 2015, **502**, 70-79.

72.   M.D. Stoller, S. Park, Y. Zhu, J. Anand R.S. Ruoff, *Nano Lett.*, 2008, 8, 3498-3502.

73.   W. Yuan, J. Chen and G. Shi, *Mater. Today*, 2014, 17, 77-85.

74.   V. Georgakilas, M. Otyepka, A.B. Bourlinos, V. Chandra, N. Kim, K.C. Kemp, P. Hobza, R. Zboril and K.S. Kim, *Chem. Rev.*, 2012, **112**, 6156-6214.

75.   N. Hedin, L. Andersson, L. Bergstrom and J. Yan, *Appl. Energy*, 2013, **104**, 418-433.

76.   Y. Zhu, S. Murali, W. Cai, X. Li, J.W. Suk, J.R. Potts and R.S. Ruoff, *Adv. Mater.*,2010, 22, 3906-3924.

77.   A.A. Baladin, S. Ghosh, W. Bao, I. Calizo, D. Teweldebrhan, F. Miao and C.N. Lau, *Nano Lett.*, 2008, 8, 902-907.

78. D. Prasai, J.C. Tuberquia, R.R. Harl, G.K. Jennings and K.I. Bolotin, *ACS Nano*, 2012, 6, 1102-1108.

79. S. Park and R.S. Ruoff, *Nat. Nanotechnol*., 2009, 4, 217-224.

80. W. Choi, I. Lahiri, R. Seelaboyina and Y.S. Kang, *Crit. Rev. Solid State Mater. Sci*., 2010, 35, 52-71.

81. P. Avouris and C. Dimitrakopoulos, *Mater. Today*, 2012, 15, 86-97.

82. Y. Zhang, L. Zhang and C. Zhou, *Acc. Chem.Res*., 2013, 46, 2329-2339.

83. A. Ghosh, K.S. Subrahmanyam, K.S. Krishna, S. Datta, A. Govindaraj, S.K. Pati and C.N.R. Rao, *J. Phys. Chem. C*, 2008, **112**, 15704-15707.

84. A.K. Mishra and S. Ramaprabhu, *AIP Adv*., 2011, **1**,032152.

85. Y. Wang, C. Guan, K. Wang, C.X. Guo and C.M. Li, *J. Chem. Eng. Data*, 2011, **56**, 642-645.

86. L.-Y. Meng and S.-J. Park, *J. Colloid Interface Sci*., 2012, **386**, 285-290.

87. G. Ning, C. Xu, L. Mu, G. Chen, G. Wang, J. Gao, Z. Fan, W. Qian and F. Wei, *Chem. Commun*., 2012, **48**, 6815-6817.

88. K. Xia, X. Tian, S. Fei and K. You, *Int. J. Hydrogen Energ.*, 2014, **39**, 11047-11054.

89. Z.-Y. Sui, Q.-H. Meng, J.-T. Li, J.-H. Zhu, Y. Cui and B.-H. Han, *J. Mater. Chem. A*., 2014, **2**, 9891-9898.

90. R. Kumar, V.M. Suresh, T.K. Maji and C.N.R. Rao, *Chem. Commun*., 2014, **50**, 2015-2017.

91. V. Chandra, S.U. Yu, S.H. Kim, Y.S. Yoon, D.Y. Kim, A.H. Kwon, M. Meyyappan and K.S. Kim, *Chem. Commun*., 2012, **48**, 735-737.

92. K. Christian Kemp, V. Chandra, M. Saleh and K.S. Kim, *Nanotechnology*, 2013, **24**, 235703.

93. M. Saleh, V. Chandra, K.C. Kemp and K.S. Kim, *Nanotechnology*, 2013, **24**, 255702.

94. H. Seema, K. Christian Kemp, N.K. Le, S.-W. Park, V. Chandra, J.W. Lee and K.S. Kim, *Carbon*, 2014, **66**, 320-326.

95. J. Oh, Y.-H. Mo, V.-D. Le, S. Lee, J. Han, G. Park, Y.-H. Kim, S.-E. Park and S. Park, *Carbon*, 2014, **79**, 450-456.

96. P. Tamilarasan and S. Ramaprabhu, *J. Mater. Chem. A*., 2015, **3**, 101-108.

97. D. Zhou, Q.-Yi Cheng, Y. Cui, T. Wang, X. Li and B.-H. Han, *Carbon*, 2014, **66**, 592-598.

98. A.K. Mishra and S. Ramaprabhu, *J. Mater. Chem*., 2012, **22**, 3708-3712.

99. A.K. Mishra and S. Ramaprabhu, *J. Appl. Phys*., 2014, **116**, 064306.

100. Z. Ding, L. Qing, C. QianYi, Z. YanChao, C. Yi, W. Tao and H. BaoHang, *Chin. Sci. Bull*., 2012, **57**, 3059-3064.

101. S. Yang, L. Zhan, X. Xu, Y. Wang, L. Ling and X. Feng, *Adv. Mater*., 2013, **25**, 2130-2134.

102. S.-Y. Lee and S.-J. Park, *Carbon*, 2014, **68**, 112-117.

103. G. Srinivas, J. Burress and T. Yildirim, *Energy Environ. Sci.*, 2012, **5**, 6453-6459.

104. Z.-Y. Sui and B.-H. Han, *Carbon*, 2015, **82**, 590-598.

105. S. Chowdhury, G.K. Parshetti and R. Balasubramanian, *Chem. Eng. J.*, 2015, **263**, 374-384.

106. A. Garcia-Gallastegui, D. Iruretagoyena, V. Gouvea, M. Mokhtar, A.M. Asiri, S.N. Basahel, S.A. Al-Thabaiti, A.O. Alyoubi, D. Chadwick and M.S.P. Shaffer, *Chem. Mater*., 2012, **24**, 4531-4539.

107. D. Iruretagoyena, M.S.P. Shaffer and D. Chadwick, *Adsorption*, 2014, **20**, 321-330.

108. Z.-Y. Sui, Y. Cui, J.-H. Zhu and B.-H. Han, *ACS Appl. Mater. Interfaces*, 2013, **5**, 9172-9179.

109. A.A. Alhwaige, T. Agag, H. Ishida and S. Qutubuddin, *RSC Adv*., 2013, **3**, 16011-16020.

110. T. Tsoufis, F. Katsaros, Z. Sideratou, G. Romanos, O. Ivashenko, P. Rudolf, B.J. Kooi, S. Papageorgiou and M.A. Karakassides, *Chem. Commun*., 2014, **50**, 10967-10970.

111. R. Kumar, K. Jayaramulu, T.K. Maji and C.N.R. Rao, *Chem. Commun.*, 2013, **49**, 4947-4949.

112. W. Huang, X. Zhou, Q. Xia, J. Peng, H. Wang and Z. Li, *Ind. Eng. Chem. Res.*, 2014, **53**, 11176-11184.

113. X. Zhou, W. Huang, J. Miao, Q. Xia, Z. Zhang, H. Wang and Z. Li, *Chem. Eng. J.*, 2015, **266**, 339-344.

114. Y. Cao, Y. Zhao, Z. Lv, F. Song and Q. Zhong, *J. Ind. Eng. Chem*., 2015,**27**, 102-107.

115. Z. Bian, X. Zhu, T. Jin, J. Gao, J. Hu and H. Liu, *Micropor. Mesopor. Mat*., 2014, **200**, 159-164.

116. H. Wu, Q. Gong, D.H. Olson and J. Li, *Chem. Rev*., 2012, **112**, 836-868.

117. J.U. Keller and R. Staudt, *Gas Adsorption Equilibria: Experimental Methods and Adsorptive Isotherms*, Springer, Boston (USA), 2005.

118. M. Thommes, *Chem. Ing. Tech*., 2010, **82**, 1059-1073.

119. D.P. Broom, in *Carbon Nanomaterials For Gas Adsorption*, ed. M.L. Terranova, S. Orlanducci and M. Rossi, CRC Press – Taylor & Francis Group, Florida (USA), 2012, pp. 1-38.

120. A.L. Myers, *Pure Appl. Chem.*, 1989, **61**, 1949-1953.

121. L. Jiang and Z. Fan, *Nanoscale*, 2014, **6**, 1922-1945.

122. W. Yuan, J. Chen and G. Shi, *Mater. Today*, 2014, **17**, 77-85.

123. V. Presser, J. McDonough, S-H. Yeon and Y. Gogotsi, *Energy Environ. Sci.*, 2011, **4**, 3059-3066.

124. M.E. Casco, M. Martinez-Escandell, J. Silvestre-Albero, F. Rodriguez-Reinoso, *Carbon*, 2014, **67**, 230-235.

125. W. Xing, C. Liu, Z. Zhou, L. Zhang, J. Zhou, S. Zhou, Z. Yan, H. Gao, G. Wang and S.Z. Qiao, *Energy Environ. Sci.*, 2012, **5**, 7323-7327.

126. Y. Zhao, H. Ding and Q. Zhong, *Appl. Surf. Sci.*, 2012, **258**, 4301-4307.

127. R. Kumar, K. Jayaramulu, T.K. Maji and C.N.R. Rao, *Dalton Trans.*, 2014, **43**, 7383-7386.

128. J.-R. Li, Y. Ma, M.C. McCarthy, J. Sculley, J. Yu, H.-K. Jeong, P.B. Balbuena and H.-C. Zhou, *Coord. Chem. Rev.*, 2011, **255**, 1791-1823.

129. R.B. Getman, Y.-S. Bae, C.E. Wilmer and R.Q. Snurr, *Chem. Rev.*, 2012, **112**, 703-723.

130. P. Carbrera-Sanfelix, *J. Phys. Chem. A*, 2009, **113**, 493-498.

131. Y. Liu and J. Wilcox, *Environ. Sci. Technol.*, 2011, **45**, 809-814.

132. T. Ohba and H. Kanoh, *J. Phys. Chem. Lett.*, 2012, **3**, 511-516.

133. B.C. Wood, S.Y. Bhinde, D. Dutta, V.S. Kandagal, A.D. Pathak, S.N. Punnathanam, K.G. Ayappa and S. Narasimhan, *J. Chem. Phys.*, 2012, **137**, 054702.

134. T. Dasgupta, S.N. Punnathanam and K.G. Ayappa, *Chem. Eng. Sci.*, 2015, **121**, 279-291.

135. I. Carrillo, E. Rangel and L.F. Magana, *Carbon*, 2009, **47**, 2752-2760.

136. C. Cazorla, S.A. Shevlin and Z.X. Guo, *J. Phys. Chem. C*, 2011, **115**, 10990-10995.

137. C. Chen, K. Xu, X. Ji, L. Miao and J. Jiang, *Phys. Chem. Chem. Phys.*, 2014, **16**, 11031-11036.

138. A.P. Terzyk, S. Furmaniak, P.A. Gauden and P. Kowalczyk, *Adsorpt. Sci. Technol.*, 2009, **27**, 281-296.

139. G. Garbergoglio, N.M. Pugno and S. Taioli, *J. Phys. Chem. C*, 2015, **119**, 1980-1987.

140. T. Yumura and A. Yamasaki, *Phys. Chem. Chem. Phys.*, 2014, **16**, 9656-9666.

141. Y. He, W. Zhou, G. Qian and B. Chen, *Chem. Soc. Rev.*, 2014, **43**, 5657-5678.

142. J.A. Mason, T.M. McDonald, T.-H. Bae, J.E. Bachman, K. Sumida, J.J. Duttin, S.S. Kaye and J.R. Long, *J. Am. Chem. Soc.*, 2015, **137**, 4787-4803.

143. O. Talu, *Chem. Ing. Tech.*, 2011, **83**, 67-82.

144. D.M. D'Alessandro, B. Smit and J.R. Long, *Angew. Chem. Int. Ed.*, 2010, **49**, 6058-6082.

Figure Captions

Fig. 1 The three main approaches to capture CO_2.

Fig. 2 Representation of the honeycomb lattice of graphene and its unit cell (indicated by the dashed line). Each unit cell comprises two equivalent sub-lattices of carbon atoms, joined together by σ bonds with a C—C bond length of 0.142 nm.

Fig. 3 Top: Schematic of the preparation of GNPs. Reprinted from Meng and Park,[86] Copyright 2012, with permission from Elsevier Ltd. Bottom: SEM images of HPG synthesized by CO_2 activation of GO at 850 ^{o}C (a, b) and 950 ^{o}C (c). Reprinted from Xia *et al*.,[88] Copyright 2014, with permission from Elsevier Ltd.

Fig. 4 SEM images and pore size distribution of (a and c) N-doped & (b and d) S-doped graphene fabricated through KOH activation of rGO/polyindole and rGO/polythiophene, respectively. Reprinted from Chandra *et al*.,[92] Copyright 2012, with permission from Royal Society of Chemistry &Seema *et al*.,[94] Copyright 2013, with permission from Elsevier Ltd.

Fig. 5(a) Illustration of the synthesis process of graphene/terpyridine complex. Reprinted from Zhou *et al*.,[97] Copyright 2013, with permission from Elsevier Ltd.

Fig. 6 FTIR spectra of graphene/Fe_3O_4 composites before and after CO_2 adsorption. The inset shows the high resolution FTIR spectra in the range 1200–2900 cm^{-1}for the CO_2-loaded composite. While peaks corresponding to =CH— (1578 cm^{-1}), >C=C (1729 cm^{-1}), —CH_2 (2850, 2918 cm^{-1}), —OH (3433 cm^{-1}) and Fe—O—Fe (598 cm^{-1}) functional moieties are clearly visible prior to adsorption, the additional peaks after adsorption can be attributed to the asymmetric stretching of CO_2 (2332 cm^{-1}), O—C—O symmetric vibrational mode of bicarbonates (1384 cm^{-1}) and C—O symmetric vibrational mode of carbonates (1044, 1094

cm^{-1}), suggesting physicochemical interactions between CO_2 and graphene/Fe_3O_4. Reprinted from Mishra and Ramaprabhu,[99] Copyright 2014, with permission from American Institute of Physics.

Fig. 7 Schematic of the fabrication method of PEI/G-silica sheets. The procedure involves three steps: (1) synthesis of GO-porous silica sheets via GO as template, (2) pyrolysis of GO-porous silica sheets at 700 ^{o}C under an Ar atmosphere to produce graphene-silica sheets, (3) impregnation of PEI into graphene-silica sheets. Reprinted from Yang *et al*.,[101] Copyright 2013, with permission from John Wiley and Sons.

Fig. 8 (a) Illustration of the major steps involved in the preparation of GO-based 3D hydrogels.(b) Digital imagesand (c) CO_2/0 ^{o}C adsorption-desorption isotherm of the hydrogels obtained at different hydrothermal temperatures (solid symbols denote adsorption and open symbols denote desorption). Reprinted from Sui and Han,[104] Copyright 2014, with permission from Elsevier Ltd.

Fig. 9 Breakthrough curves of aminated GO: ■ GO/EDA, ▲ GO/DETA, ● GO/TETA. Reprinted from Zhao *et al*.,[121] Copyright 2011, with permission from Elsevier Ltd.

Fig. 10 Different modes of CO_2 chemisorption at the surface of TiO_2/GO-0.10 composite adsorbent (Labels 1 M or 2 M refer to the number of metal atoms involved in the adsorption). CO_2 is an amphoteric molecule: the carbon atom is acidic while the oxygen atoms are weakly basic. When it is adsorbed as a base, the binding mode can involve one or two oxygen atoms of CO_2 (monodentate or bidentate) and one or two Ti centers. As an acidic species, it can bind to the oxygen functionalities at the GO surface (O–C coordinated). Reprinted from Chowdhury *et al*.,[105] Copyright 2014, with permission from Elsevier Ltd.

Fig. 11 Continuous adsorption-desorption profile (adsorption temperature: 300 ^{o}C; desorption temperature: 400 ^{o}C) of activated LDH and GO/LDH (GO content = 5 wt%) normalized to the first cycle capacity. Reprinted from Garcia-Gallastegui *et al.*,[106] Copyright 2012, with permission from American Chemical Society.

Fig. 12 Schematic of the synthesis of GO/PEI porous materials (GEPM): digital images of (a) aqueous GO dispersion, (b) GO/PEI hydrogel, & (c) GEPM and representative diagram of (d) aqueous GO dispersion, (e) GO/PEI hydrogel, & (f) GEPM. (g) SEM image of the GO/PEI hydrogel with PEI to GO weight ratio of 3:1. Reprinted from Sui *et al.*,[108] Copyright 2013, with permission from American Chemical Society.

Fig. 13 Effect of GO content on BET surface area and CO_2 adsorptionof GO/chitosan hybrid aerogels at ambient conditions. Reprinted from Alhwaige*et al.*,[109] Copyright 2013, with permission from Royal Society of Chemistry.

Fig. 14 (a) Schematic of the sodalite–zeoliticZIF-8 framework showing large cavities with narrowwindows. (b) Stepwise synthesis of the GO/ZIF-8 hybrid nanocomposite with tunable morphology and transformation of hexagonal ZIF-8 nanocrystals to nanospheres upon increasing GO content. Reprinted from Kumar*et al.*,[111] Copyright 2013, with permission from Royal Society of Chemistry.

Fig. 15 (a) IAST-predicted selectivities toward CO_2 over CH_4 for equimolar CO_2/CH_4 mixtures on Cu-BTC and GO@Cu-BTC (GO content = 1 wt%) at 0 ^{o}C as a function of total bulk pressure. Reprinted from Huang *et al.*,[112] Copyright 2014, with permission from American Chemical Society. (b) Five consecutive CO_2 adsorption/desorption cycles of GO/MIL-101 at 25°C. Reprinted from Zhou *et al.*,[113] Copyright 2014, with permission from Elsevier Ltd.

Fig. 16 Illustration of the preparation of GO-IL/$Cu_3(BTC)_2$ composites. Reprinted from Bian *et al.*,[115] Copyright 2014, with permission from Elsevier Ltd.

Fig. 17(a), (b) and (c) represent the three initial configurations considered for the physisorption of CO_2 on defected graphene sheet. In the first configuration (a), the CO_2 molecule has an initial height of 2.5 Å with its molecular axis parallel to the graphene surface. In the second configuration (b), CO_2 is still parallel to the surface but rotated 30° with respect to the structure. In the third configuration (c), the molecule is perpendicularly oriented to the surface. The optimized physisorption state is shown in (d) while the chemisorption of CO_2 as a lactone complex on the vacancy defect of the graphene layer is shown in (e). Reprinted from Cabrera-Sanfelix,[130] Copyright 2009, with permission from American Chemical Society.

Fig. 18(a) Binding energies of CO_2 and N_2 on functionalized benzenes obtained using *ab initio* calculations with MP2 theory. (b) Heats of adsorption from single component GCMC simulations at 1 bar for functionalized graphene nanoribbon bilayers with six functional groups per edge. Reprinted from Dasgupta *et al.*,[134] Copyright 2014, with permission from Elsevier Ltd.

Fig. 19 Adsorption of CO_2 onto C_2Ti system — represented by a hexagonal unit cell consisting of four Ti atoms and eight C atoms (a). When the linear CO_2 molecule approaches the C_2Ti surface, it first dissociates into CO and O. The CO fraction is then adsorbed on the surface in a manner that the C atom is bonded to three Ti atoms while the O atom is bonded to another Ti atom (b). Reprinted from Carrillo *et al.*,[135] Copyright 2009, with permission from Elsevier Ltd.

Fig. 20 CO_2 capture geometry optimized structures for (a) pristine graphene (b) Ca-doped graphene at 12.5%, and (c) Ca-doped graphene at 16.67%. Reprinted from Cazorla *et al*.,[136] Copyright 2011, with permission from American Chemical Society.

Fig. 21 Three-dimensional (3D) superstructure of PGOF. C, O and H atoms are represented respectively by green, red, and white. Reprinted from Garberoglio *et al*.,[139] Copyright 2014, with permission from American Chemical Society.

Fig. 22 Key research priorities for further development of graphene-based CO_2 adsorbents.
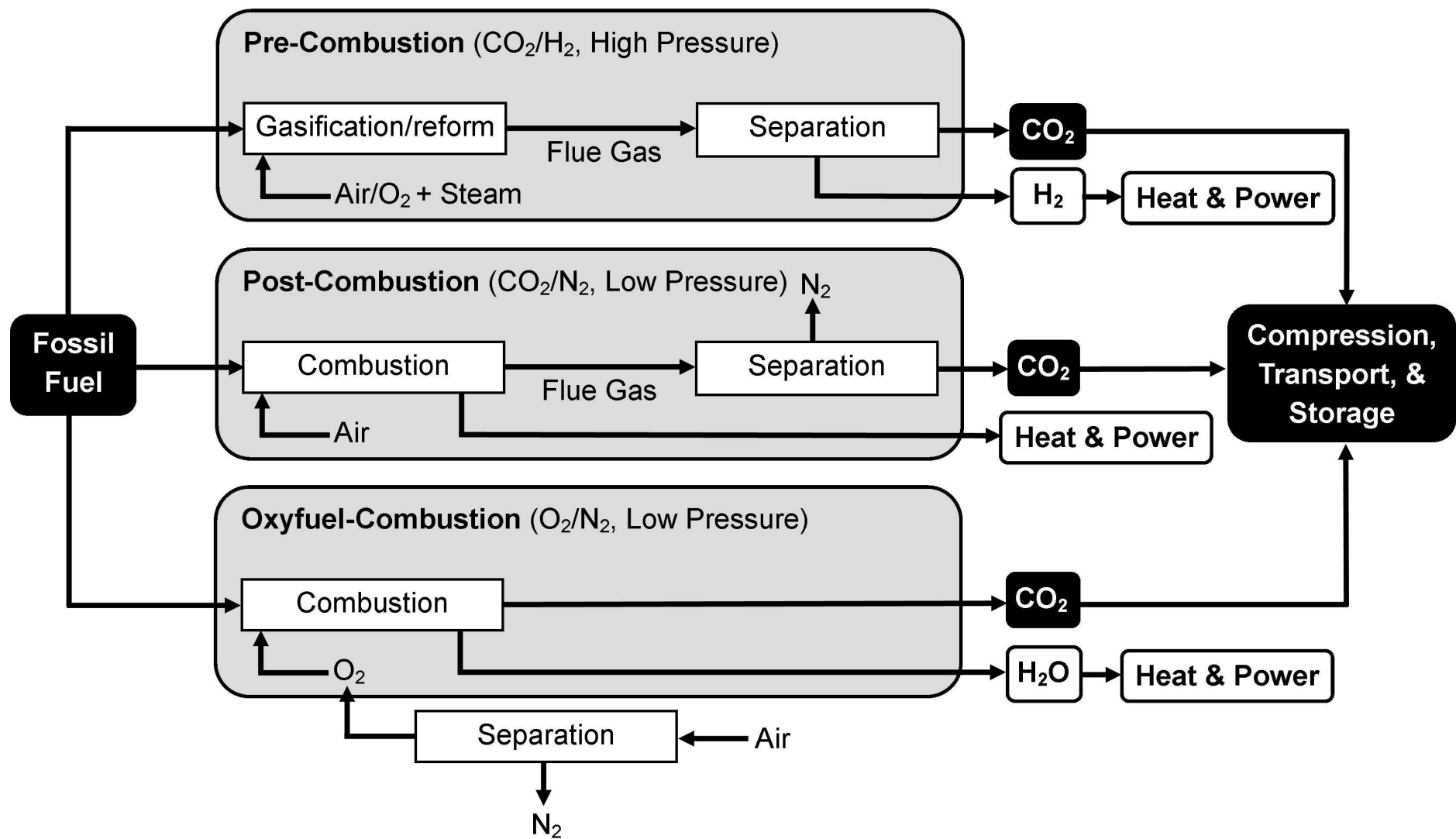
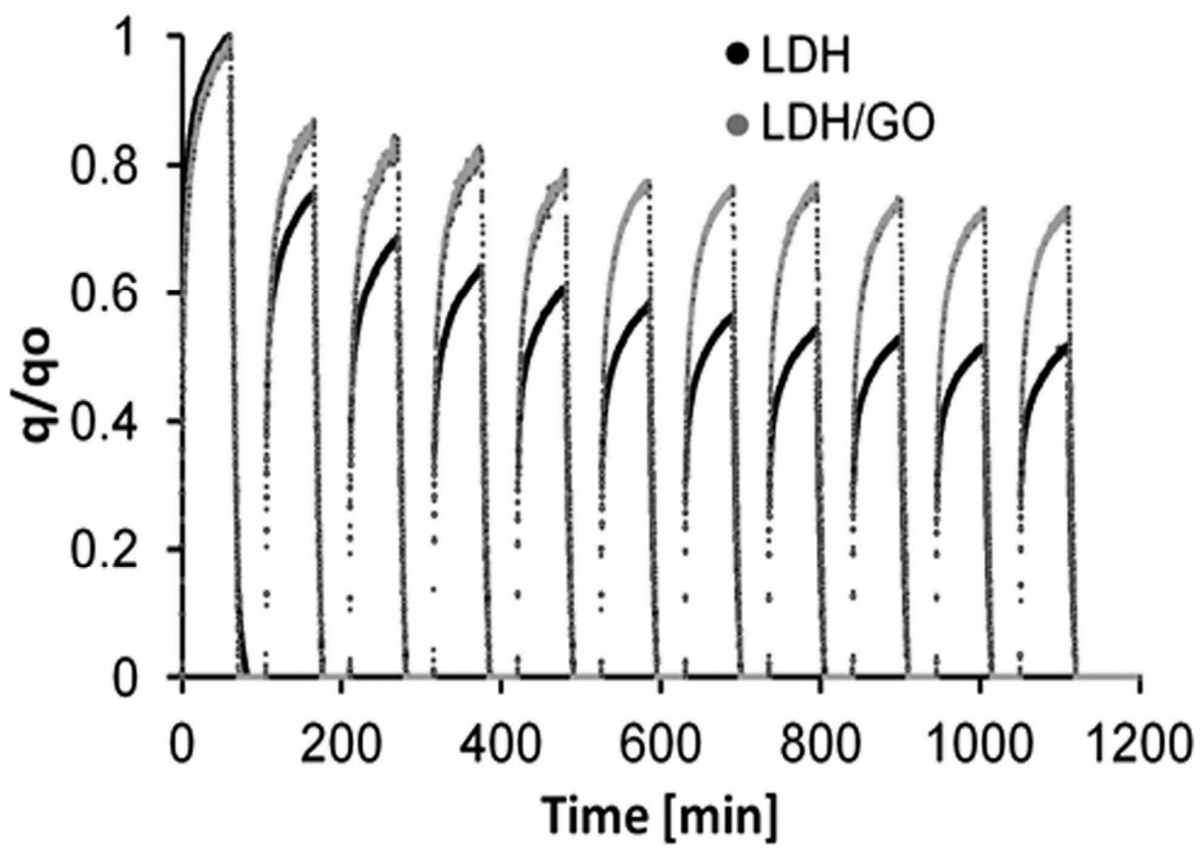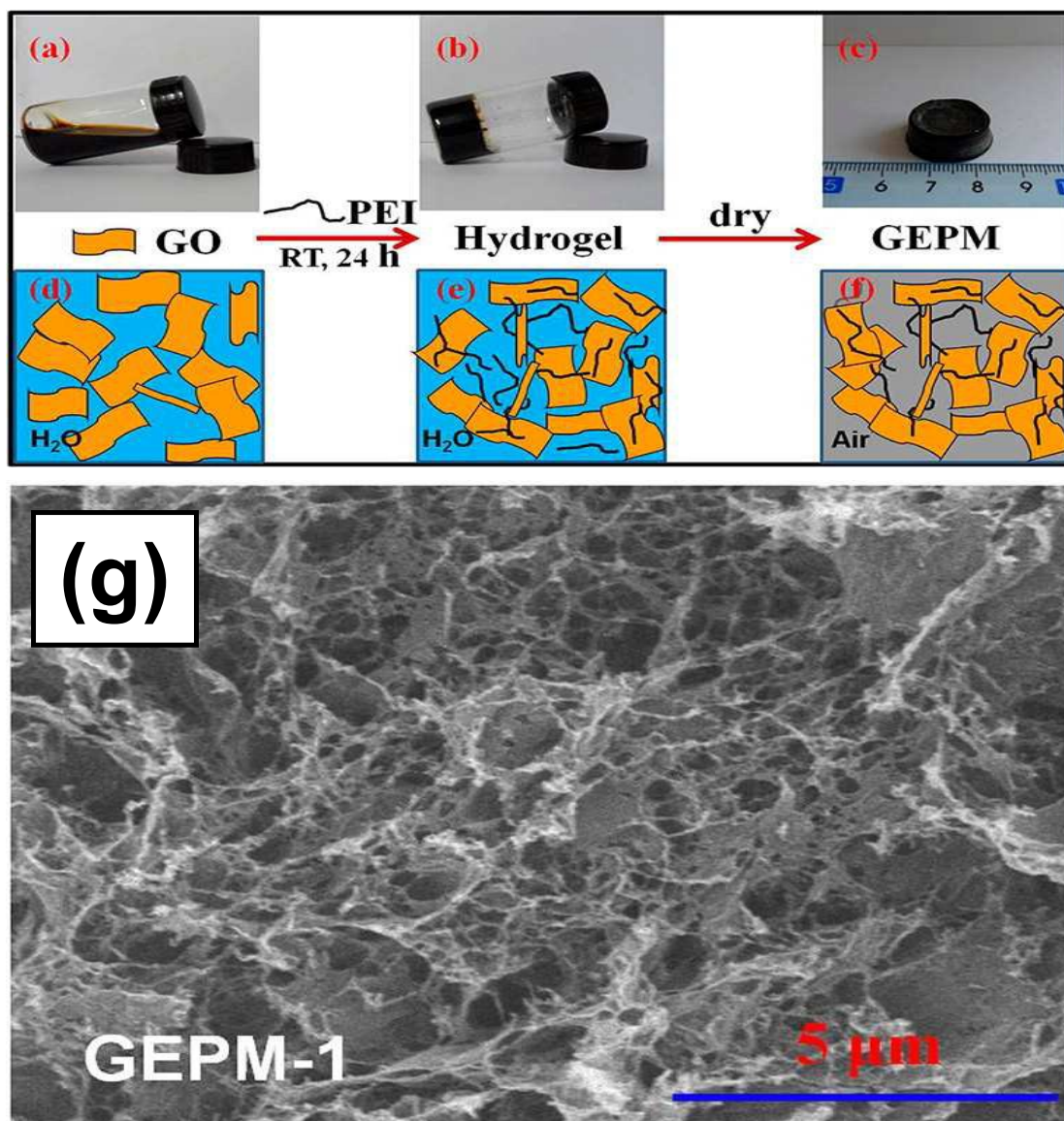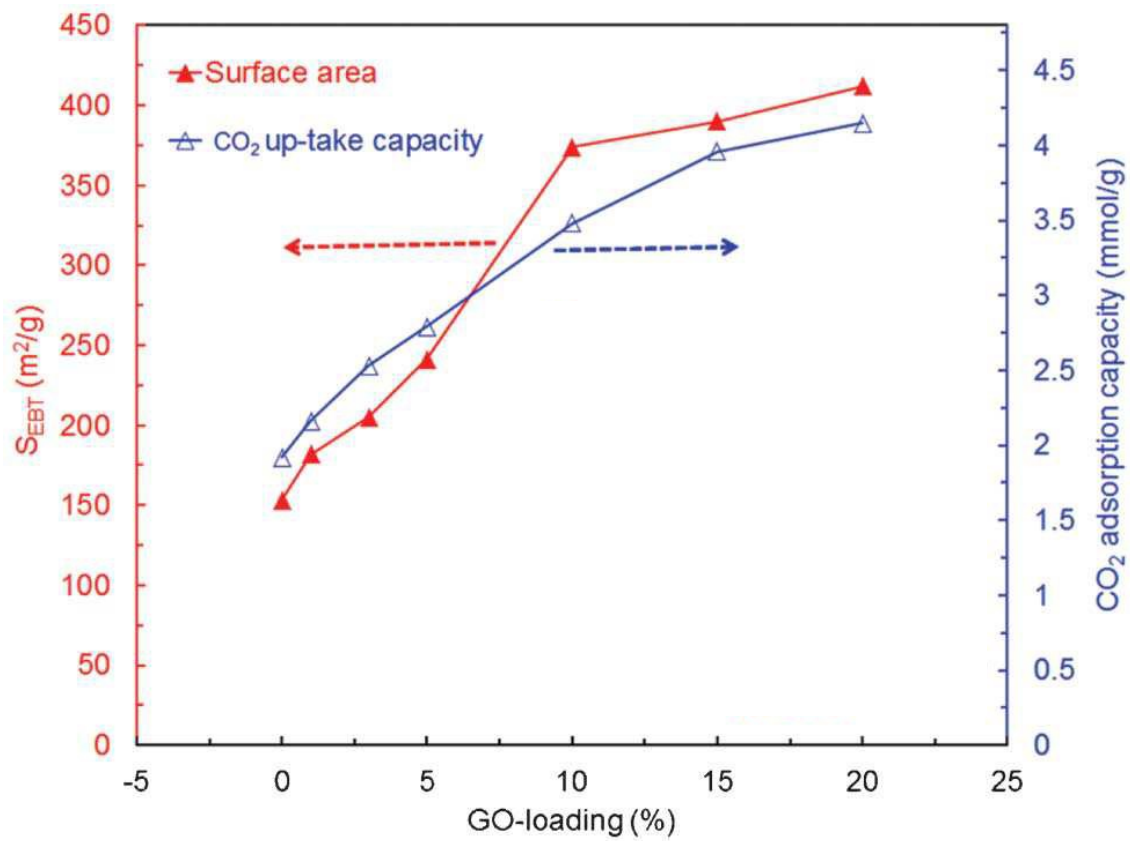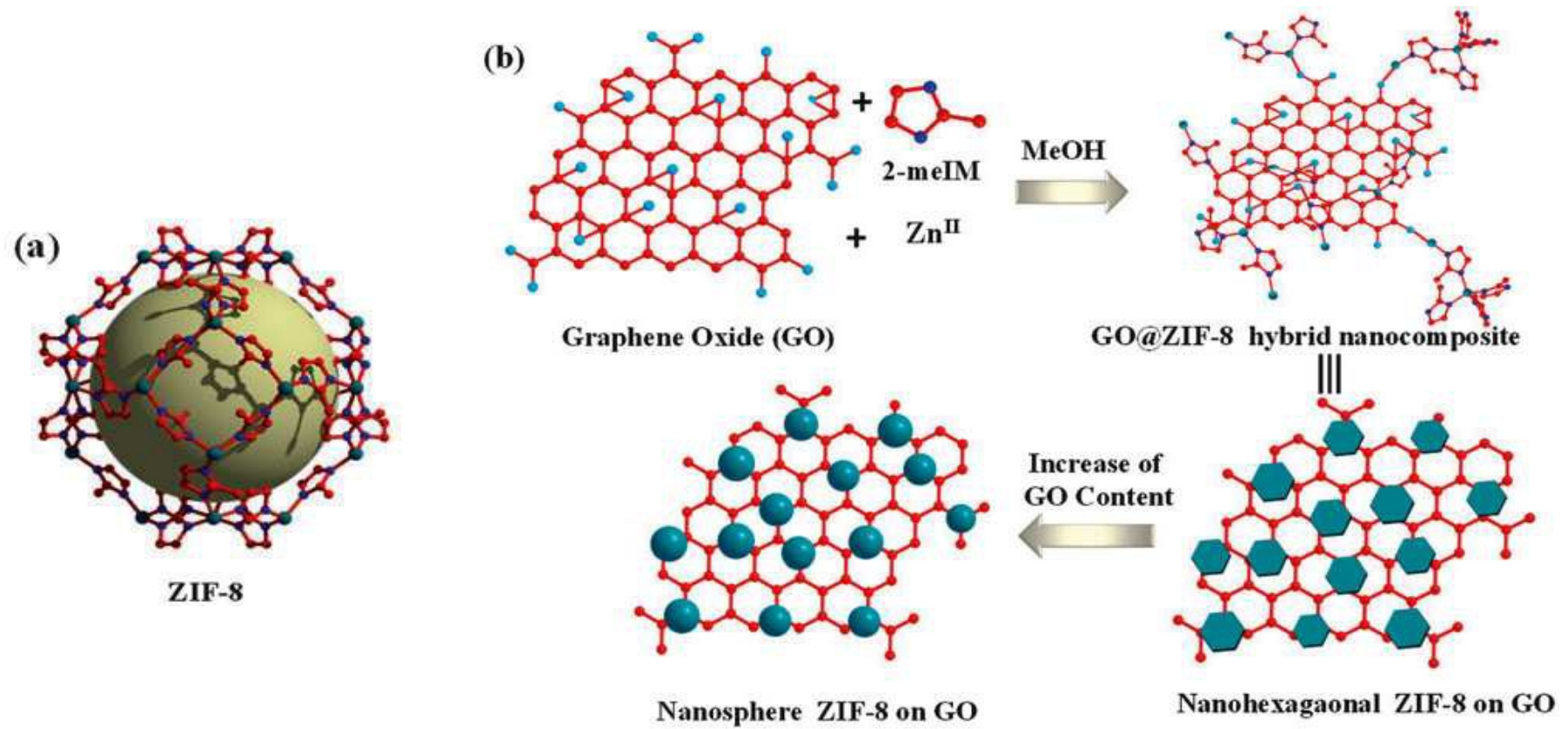Figure 1
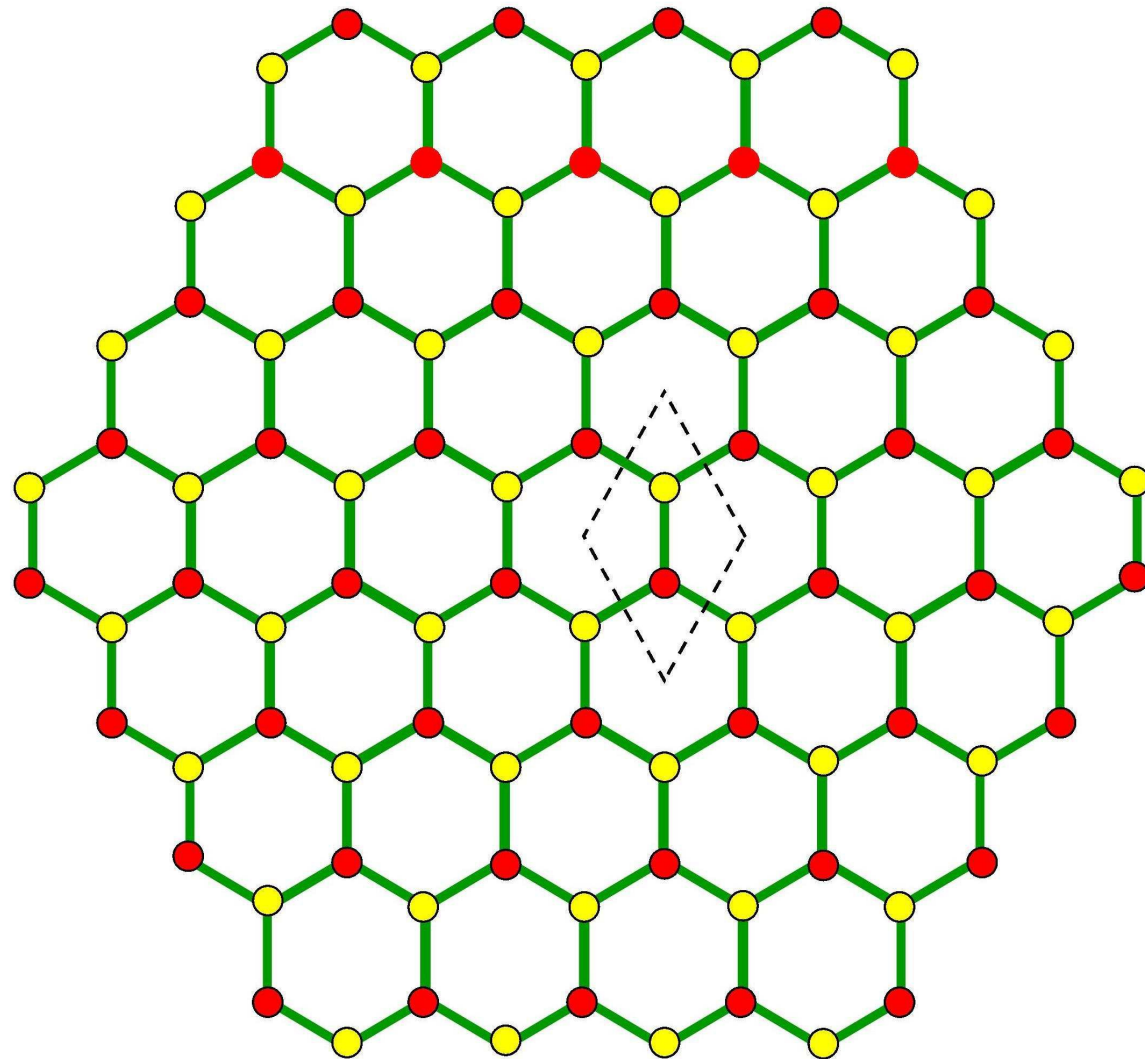
Figure 2

Figure 3

Figure 4

GO →(Carboxylation)→ **GO–COOH** →(Alkynylation)→ **Alkynyl–GO**
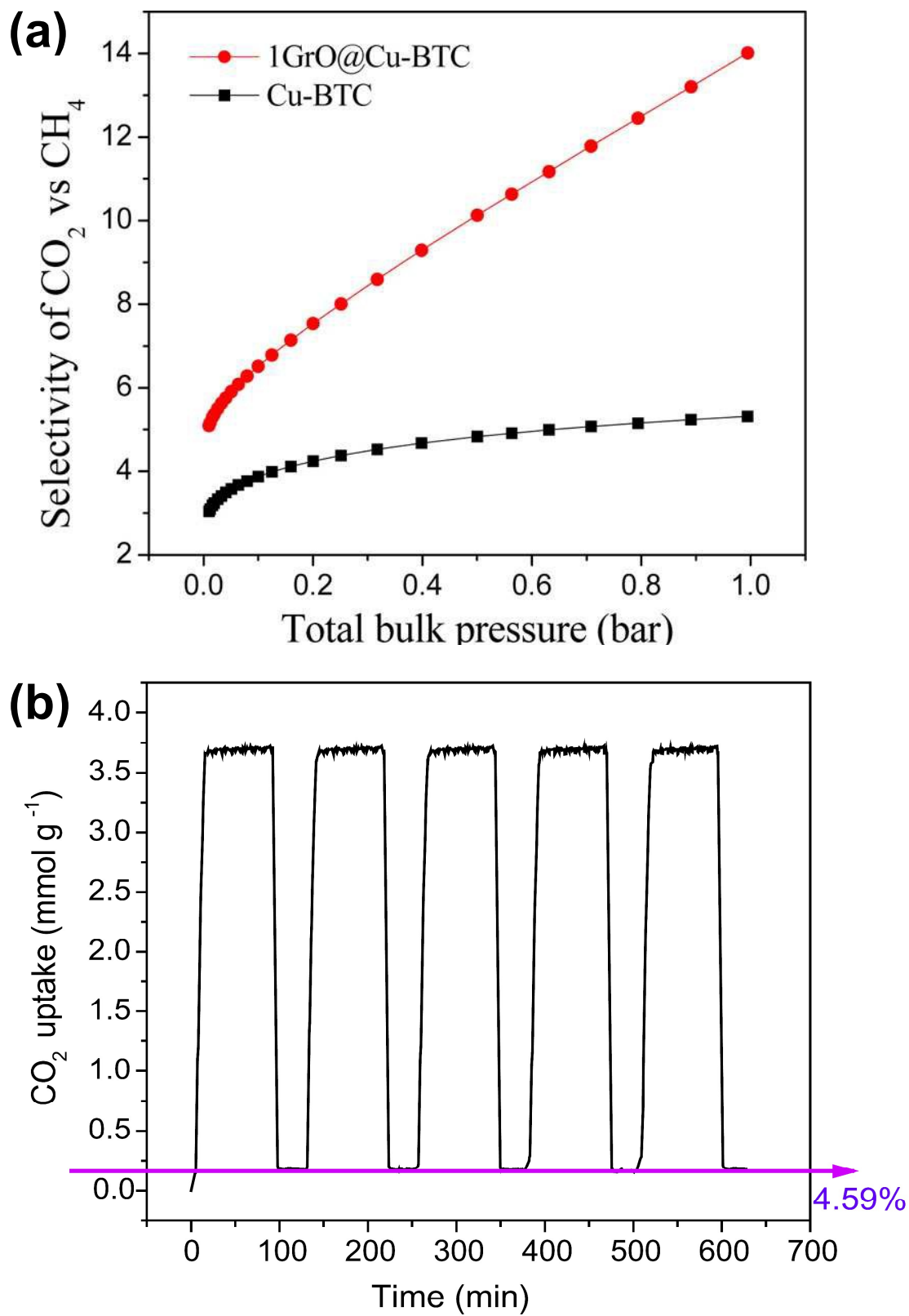
(Azido-tpy)$_2$Fe(II)

Graphene

Graphene/terpyridine complex

Click Reaction
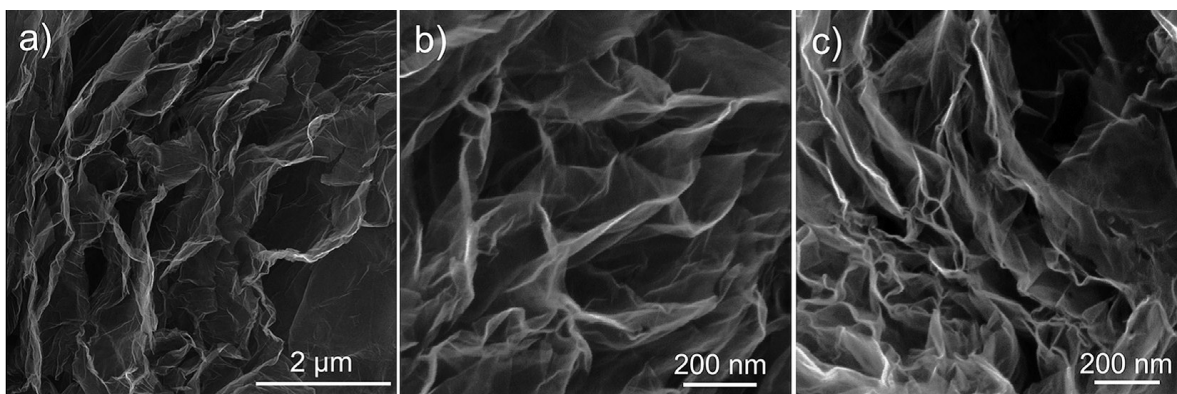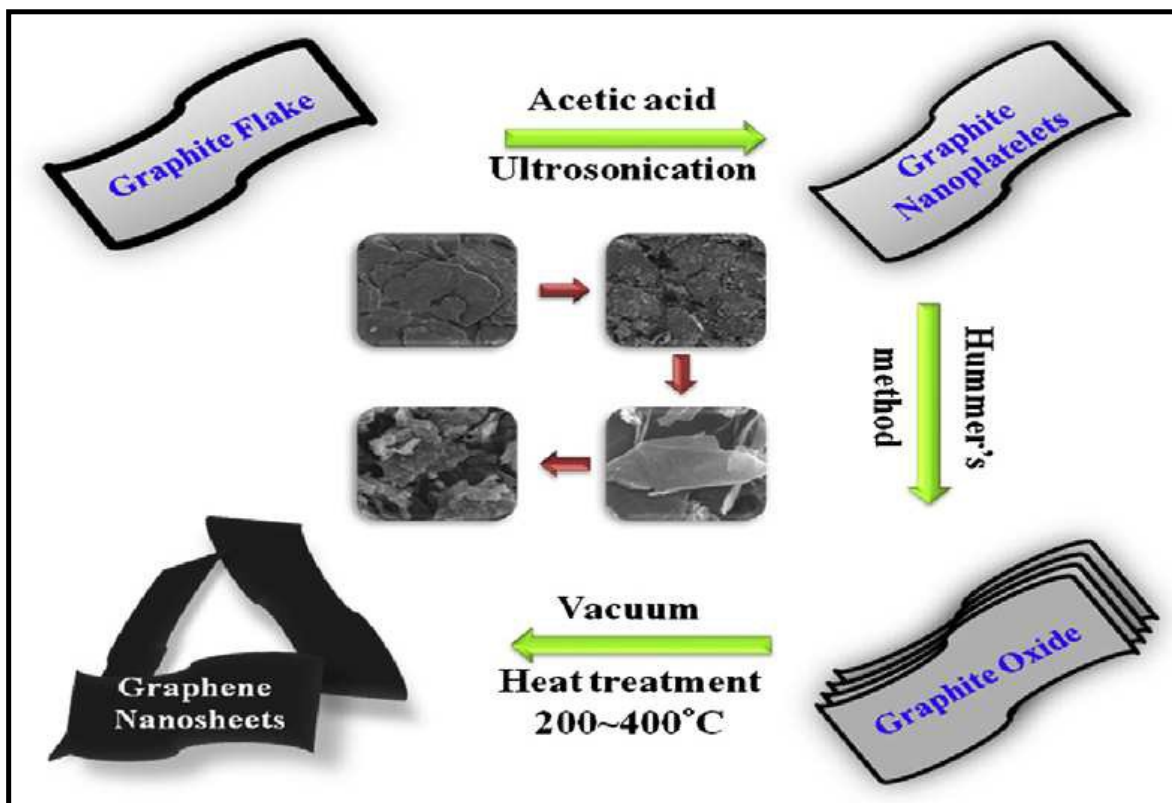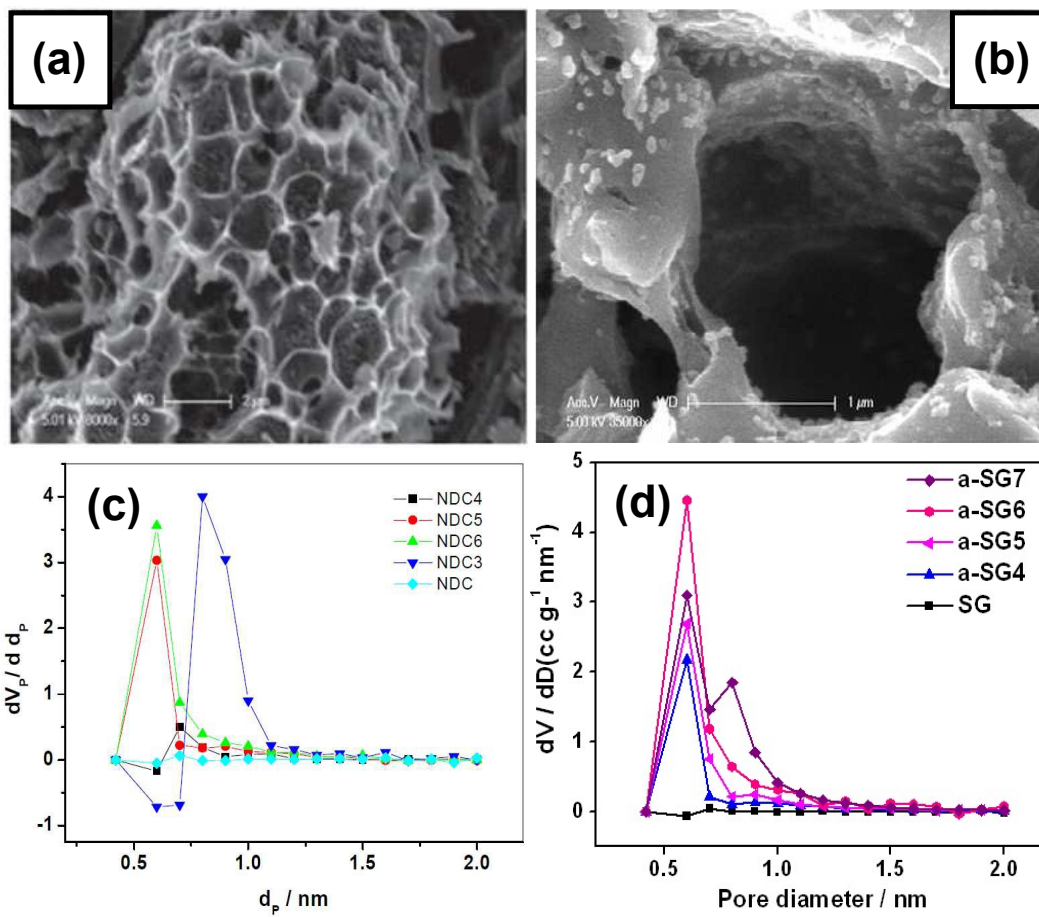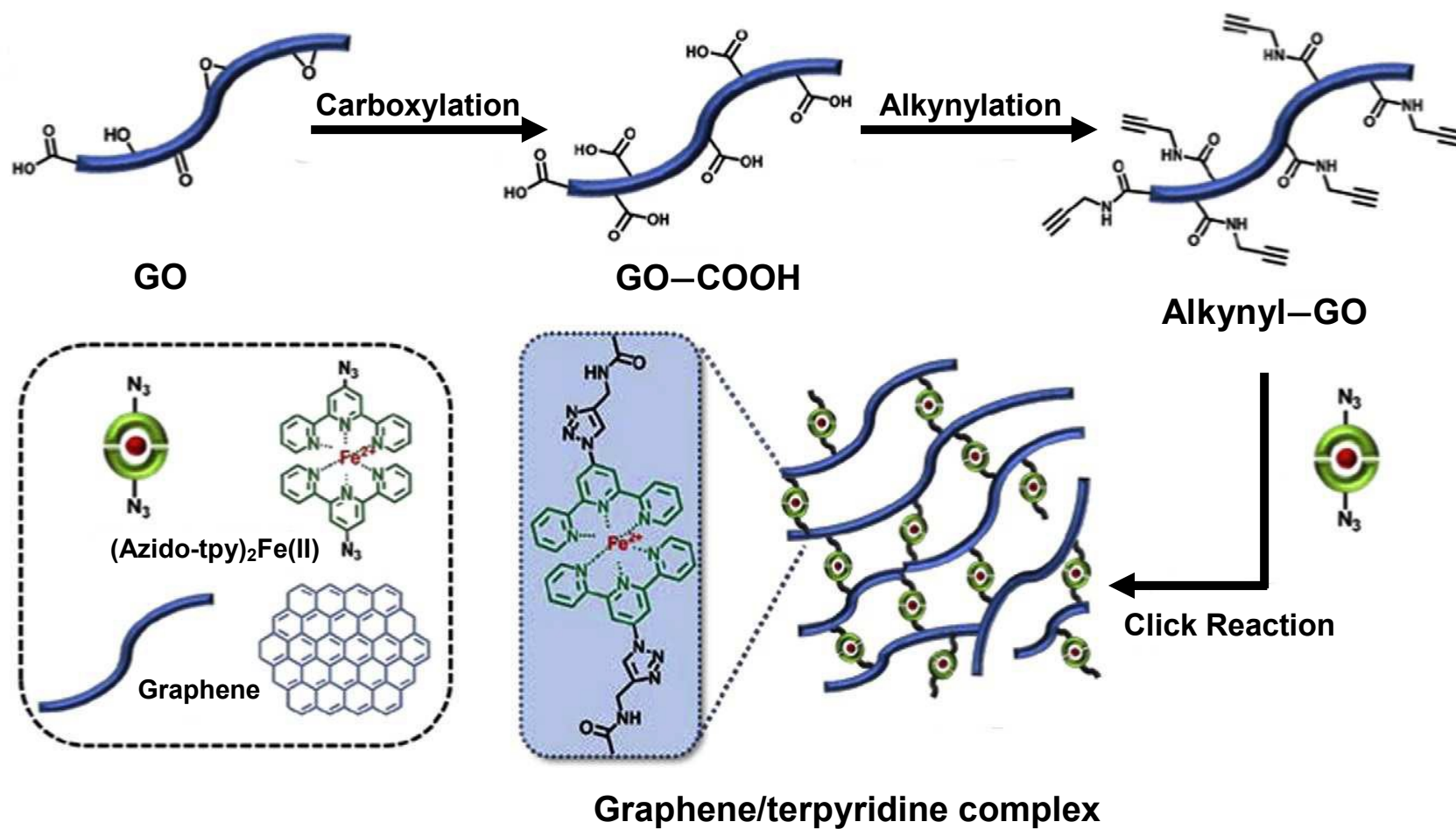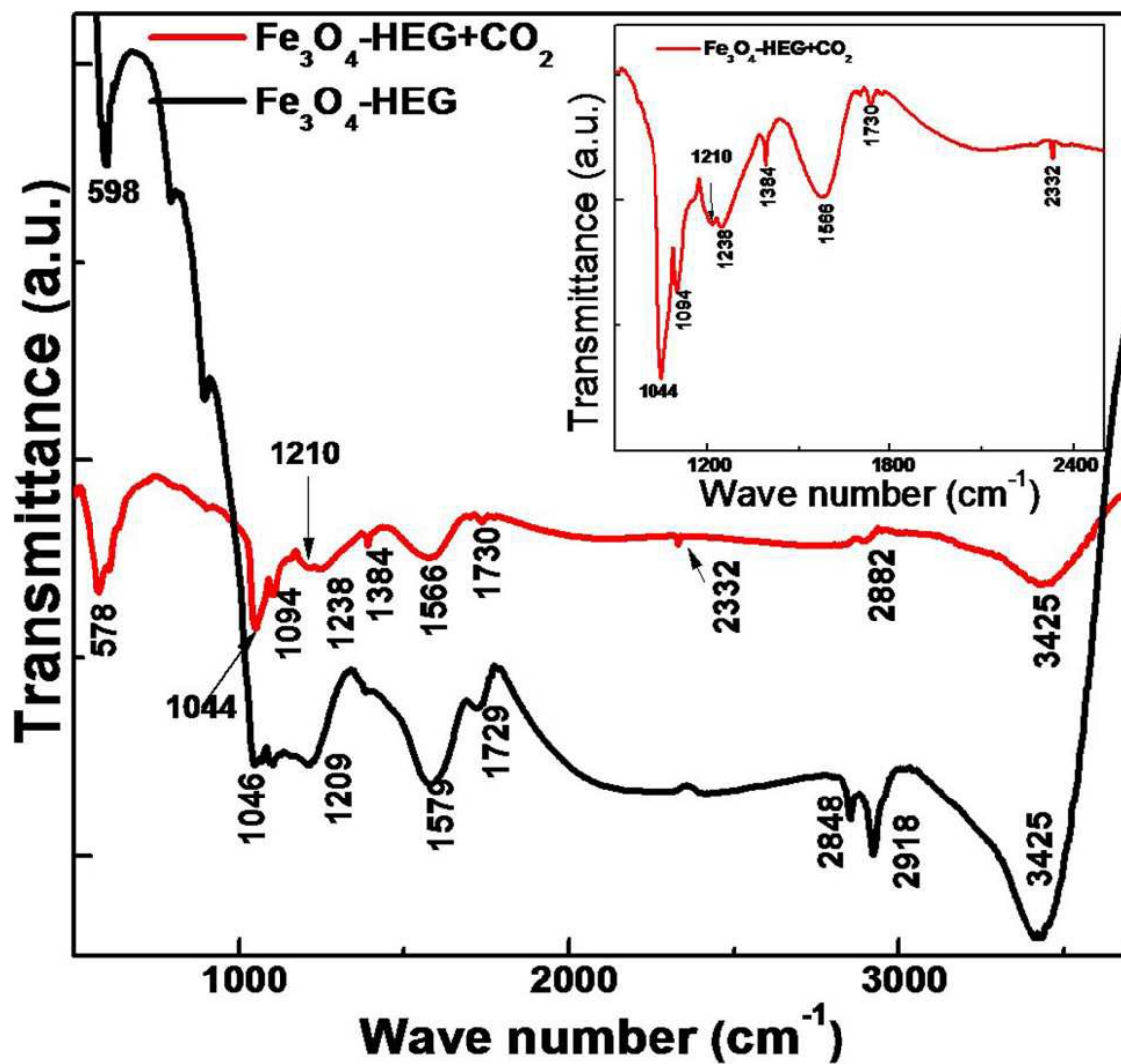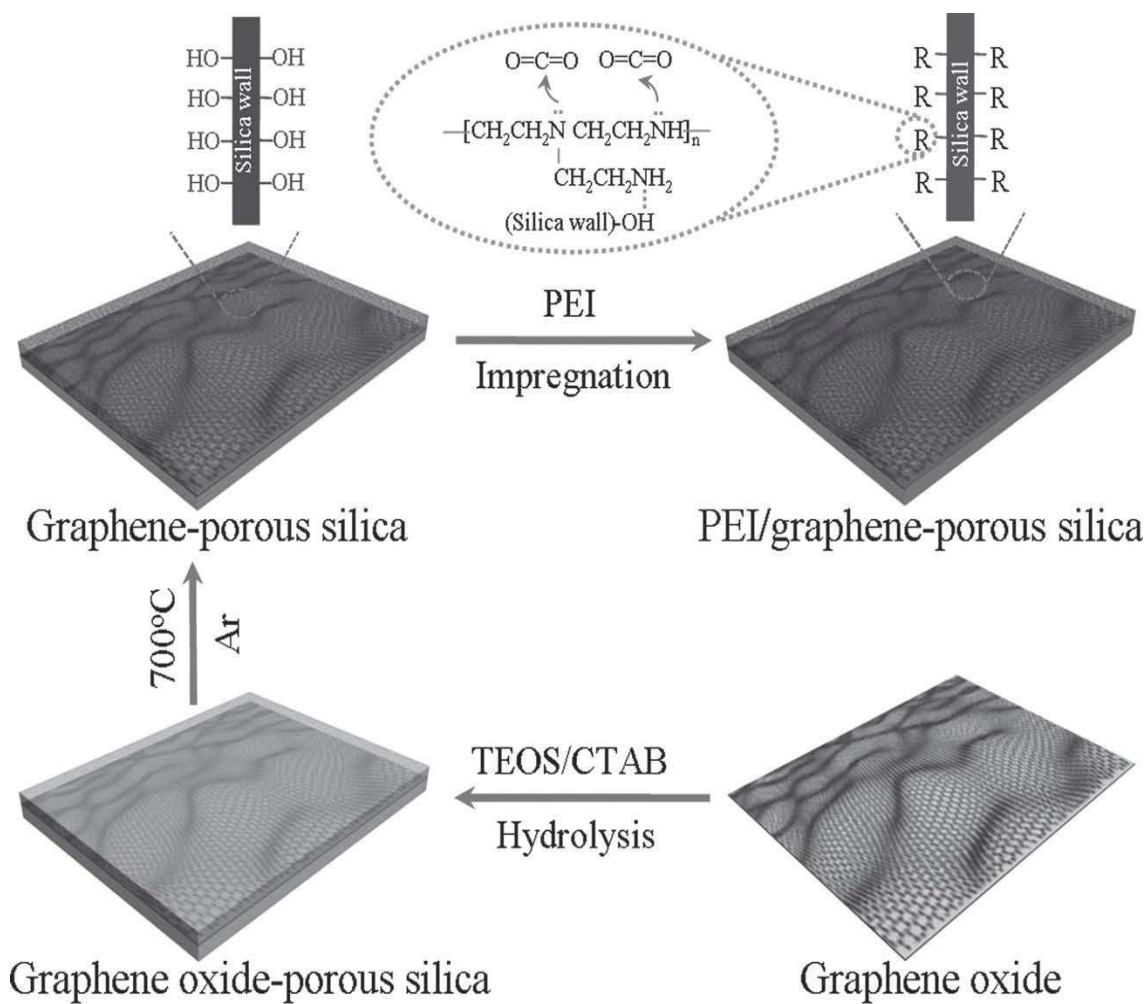
Figure 5

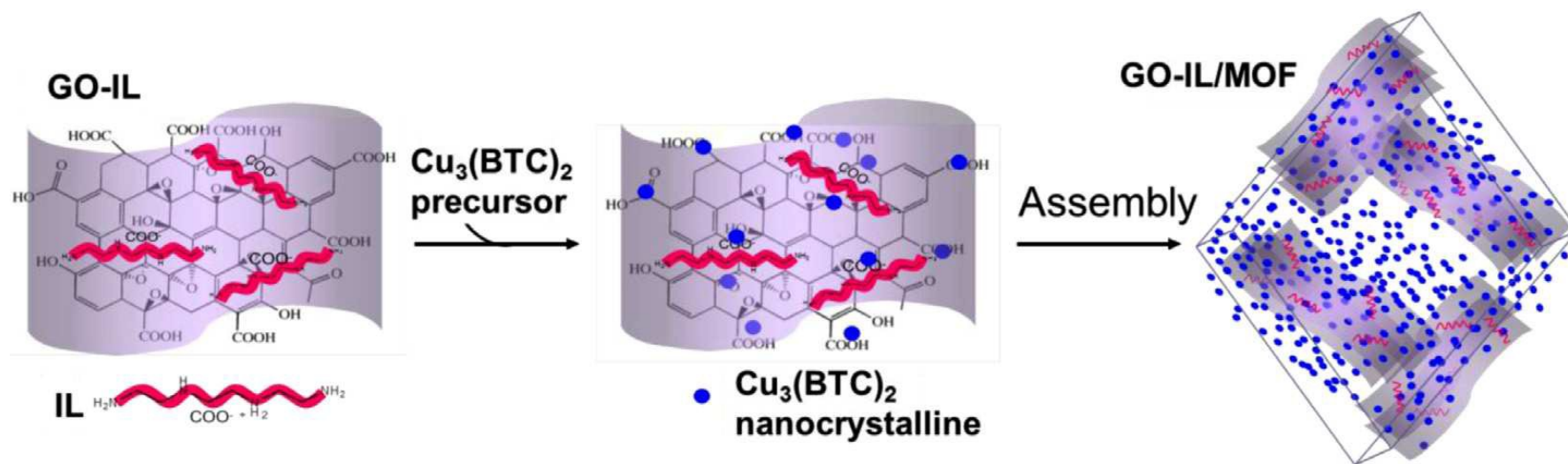Figure 6

Figure 7

Figure 8

Figure 9

1M-Monodentate   **1M-Monodentate**   **2M-Bidentate**   **1M-C Coordinated**   **O-C Coordinated**
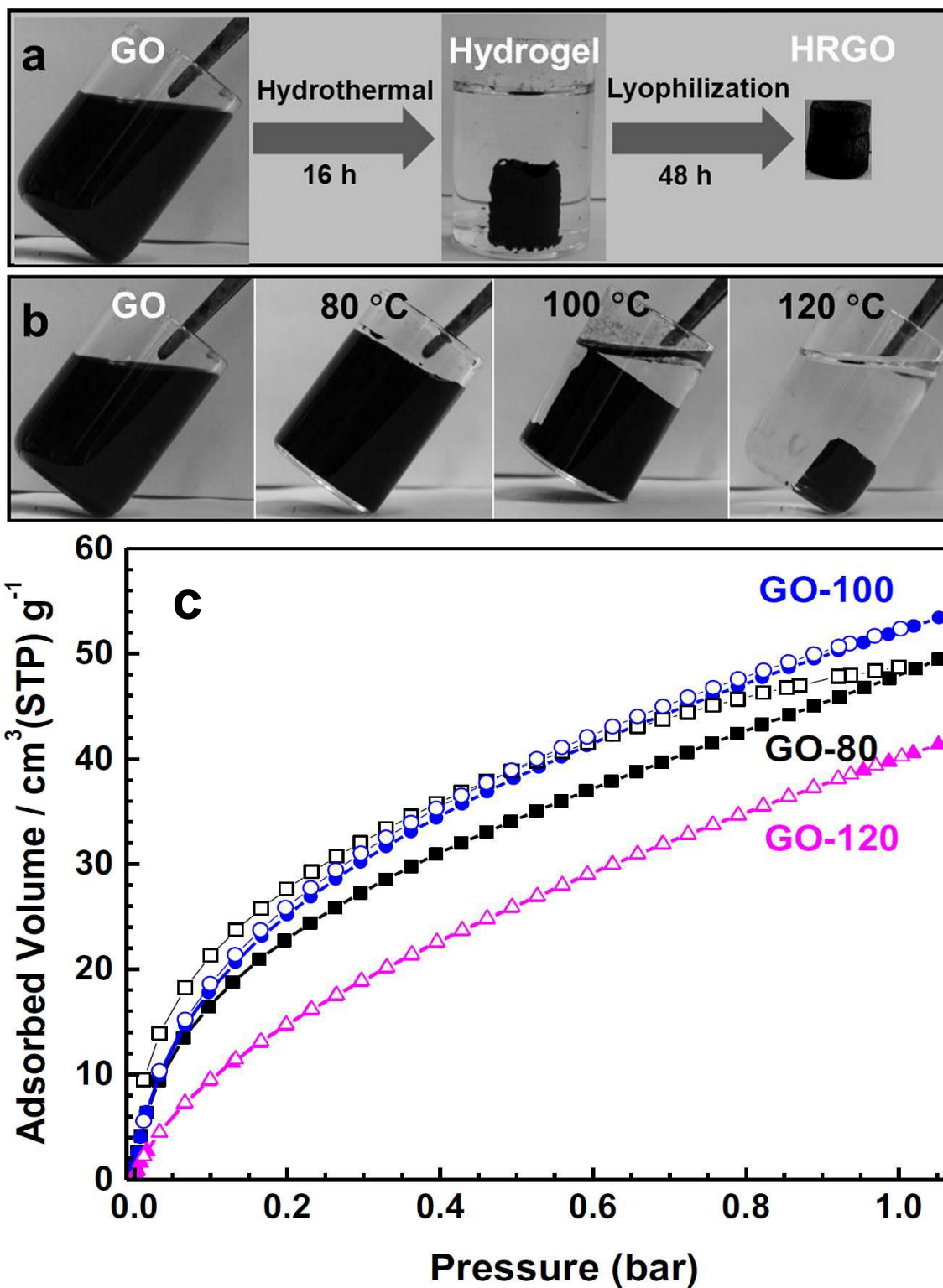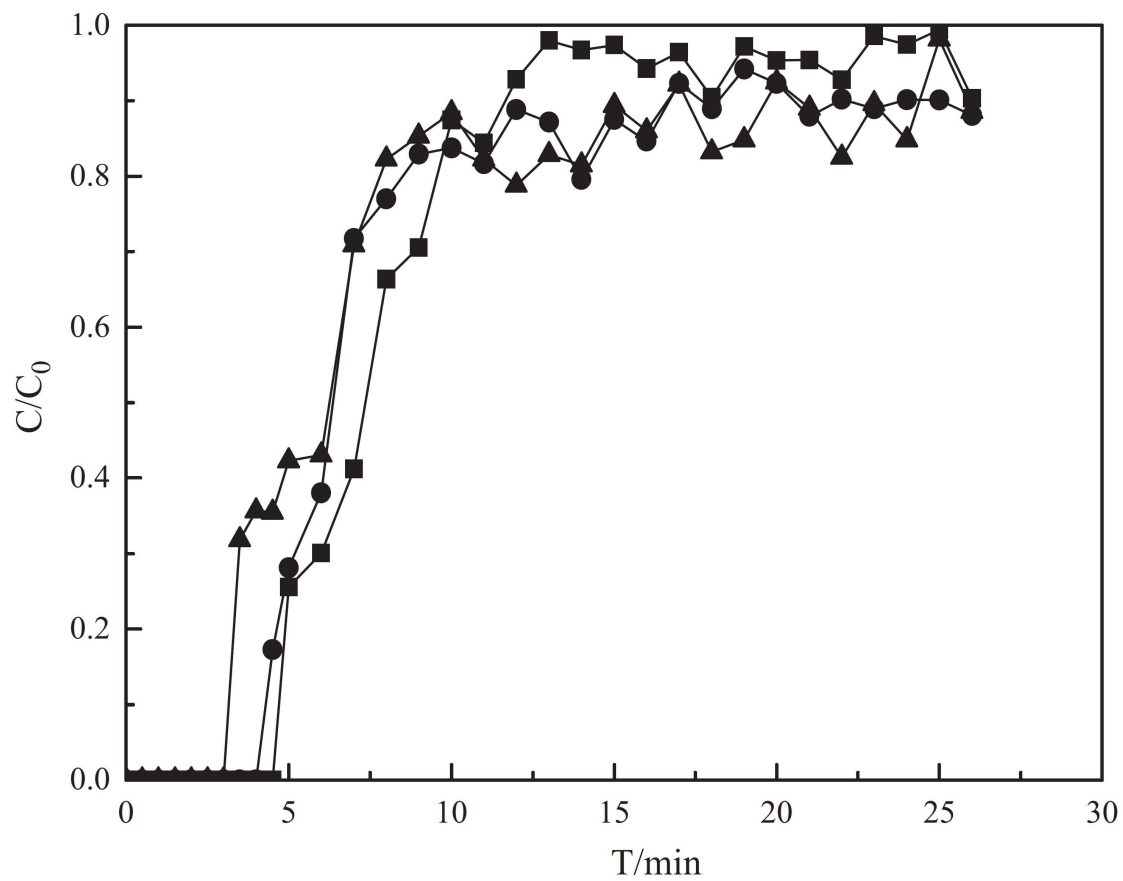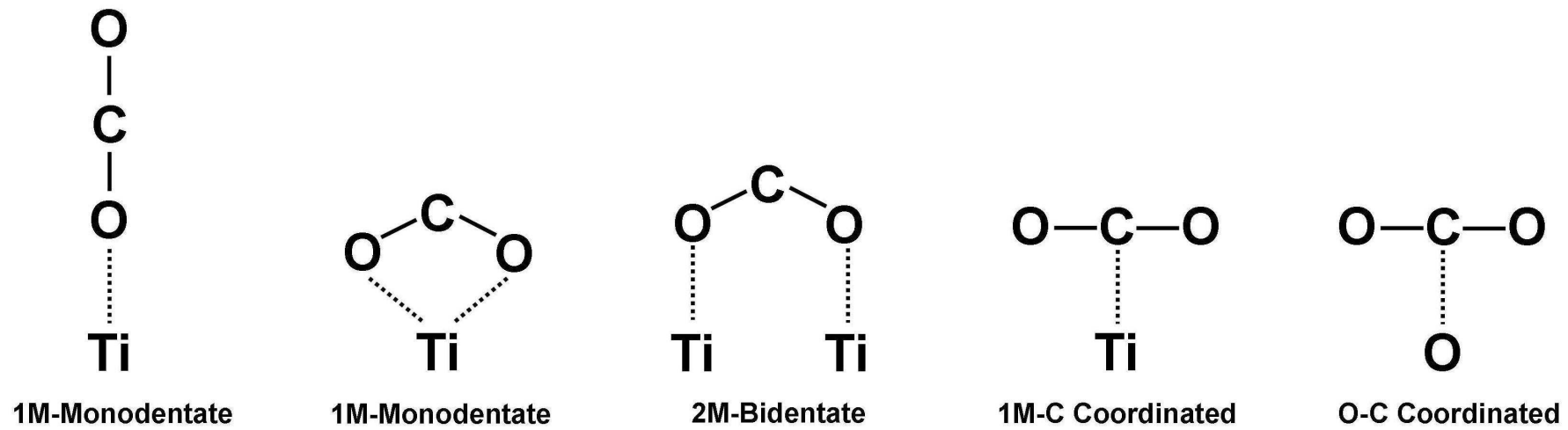
Figure 10

Figure 11

Figure 12

Figure 13

(a)

ZIF-8

(b)

Graphene Oxide (GO)

2-meIM

+ Zn^{II}

MeOH

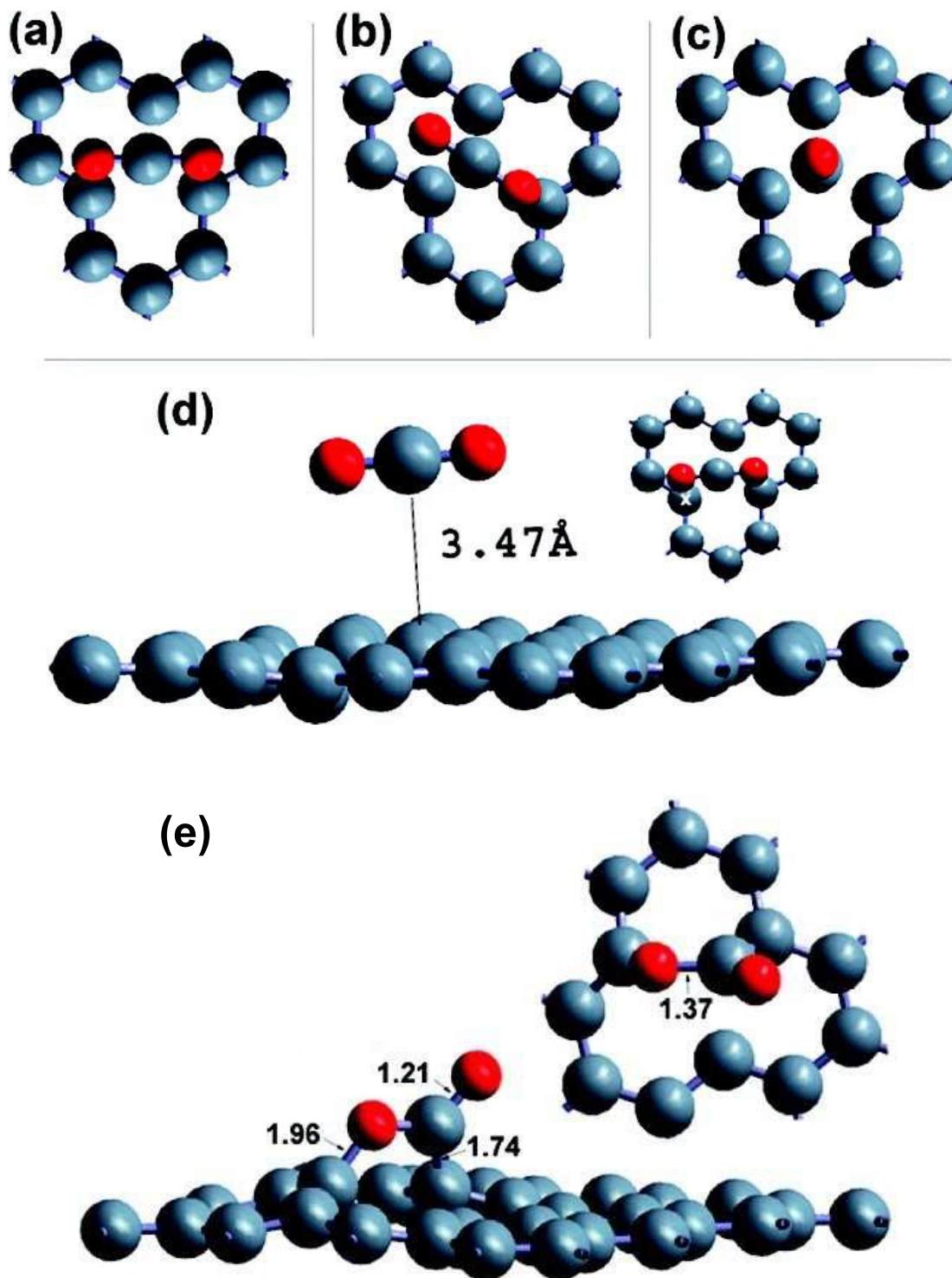GO@ZIF-8 hybrid nanocomposite

Increase of GO Content

Nanosphere ZIF-8 on GO

Nanohexagaonal ZIF-8 on GO
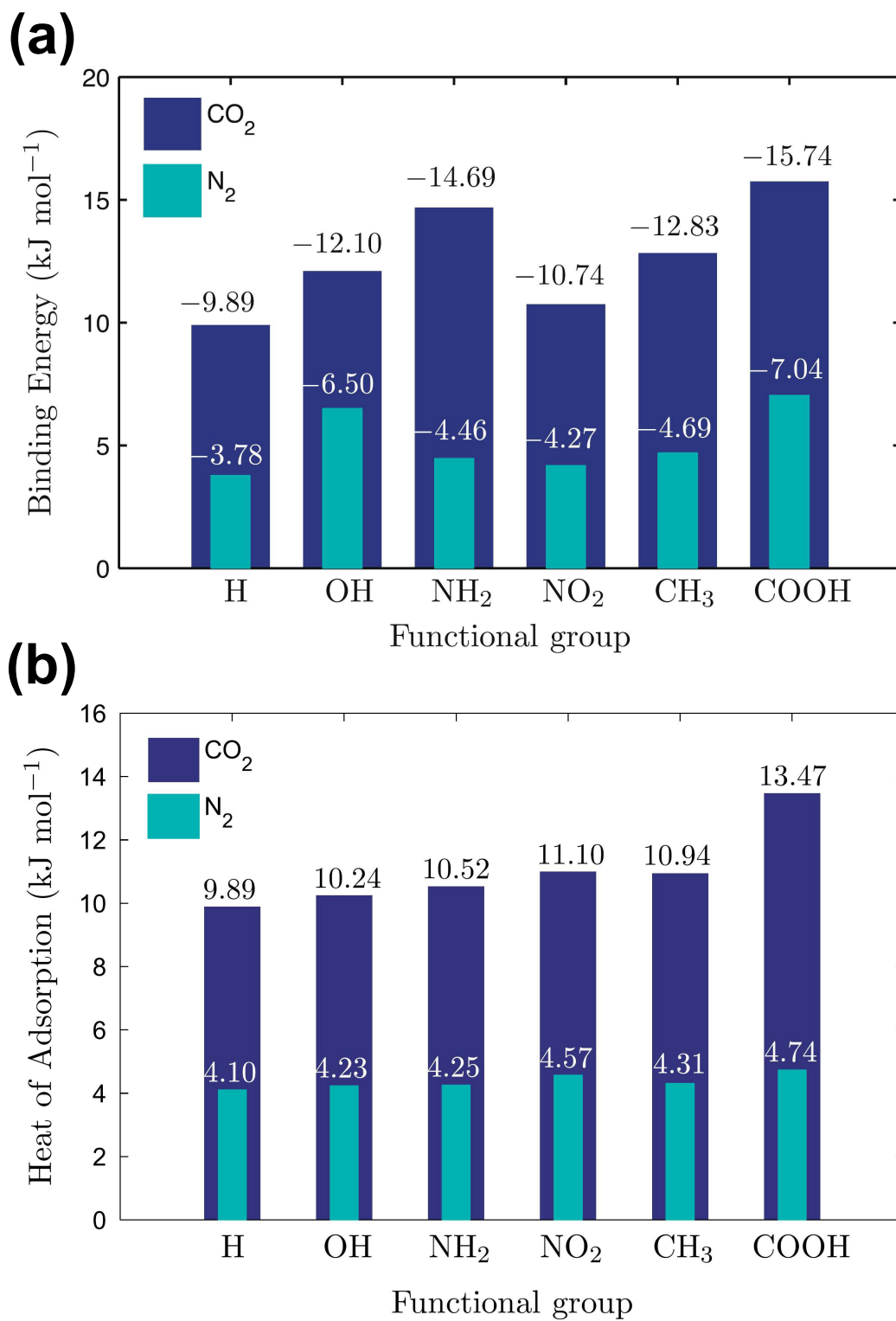
Figure 14

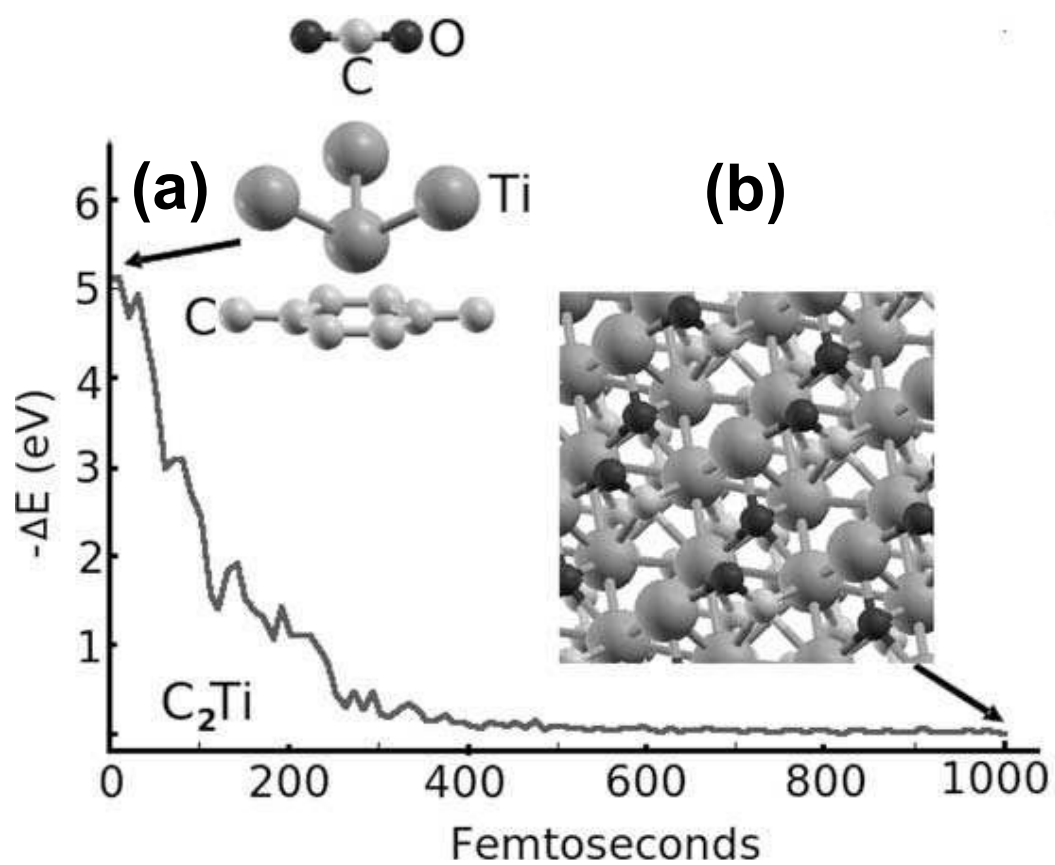Figure 15

Figure 16

Figure 17

(a)
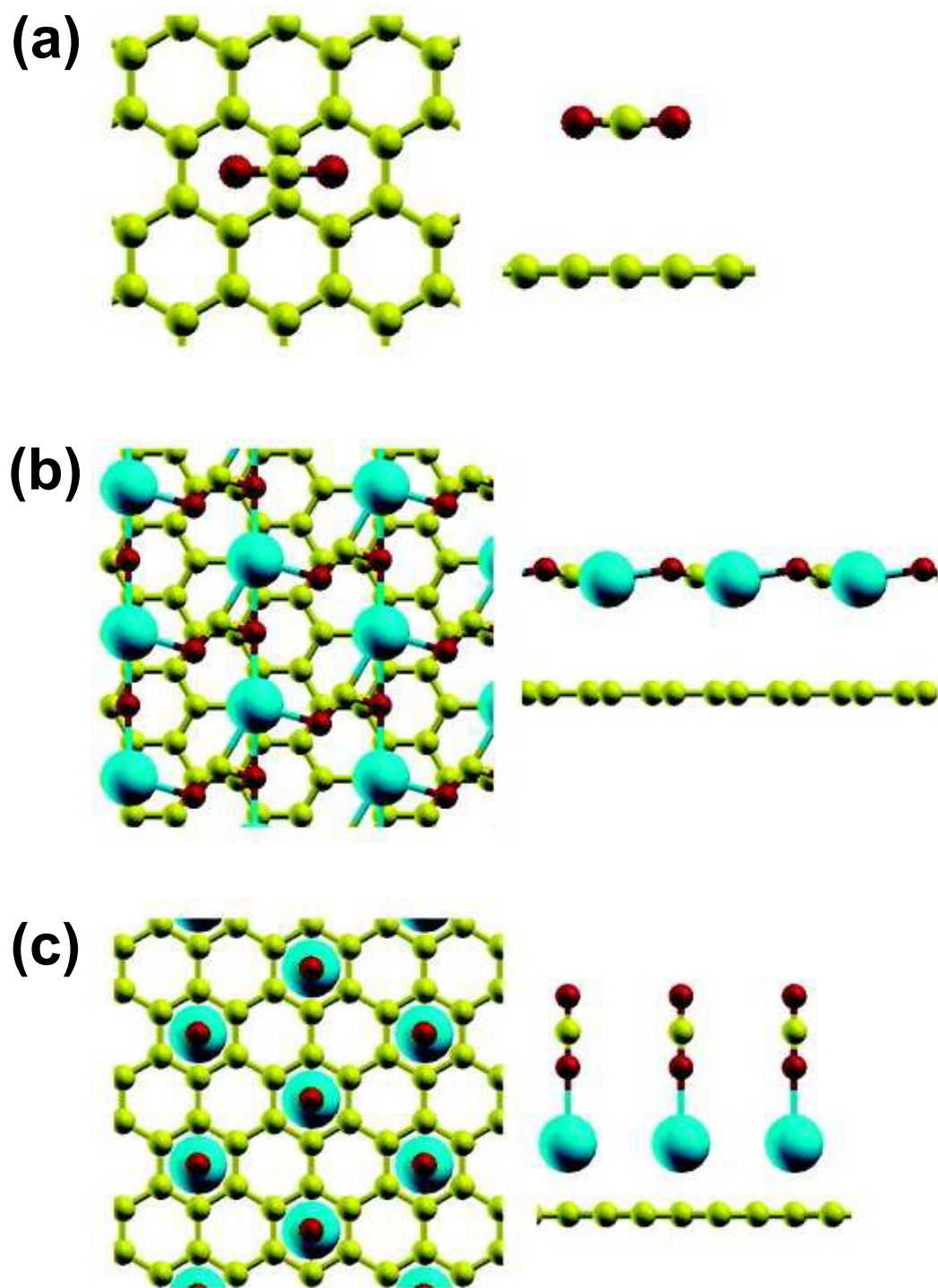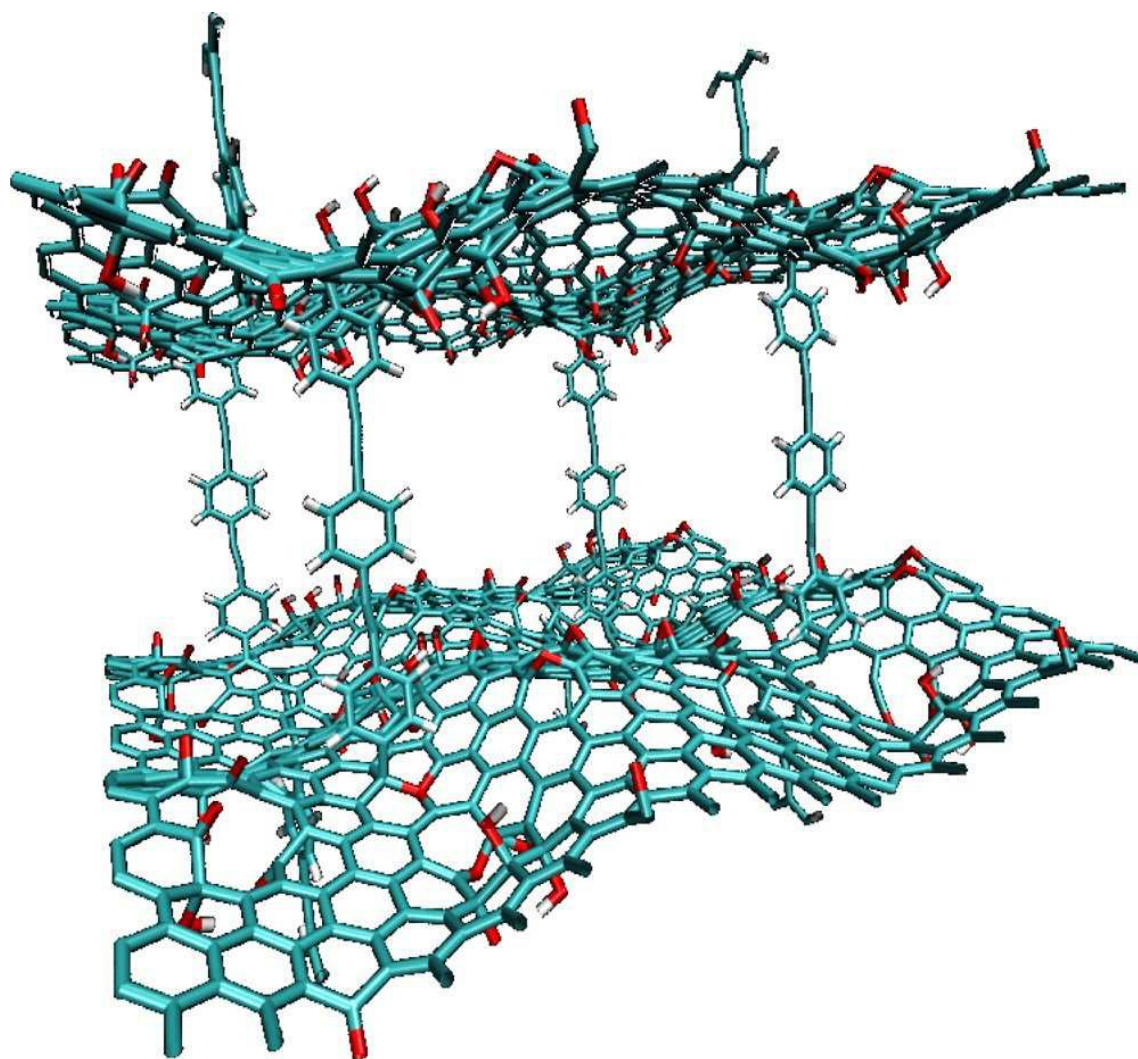

(b)

Figure 18

Figure 19
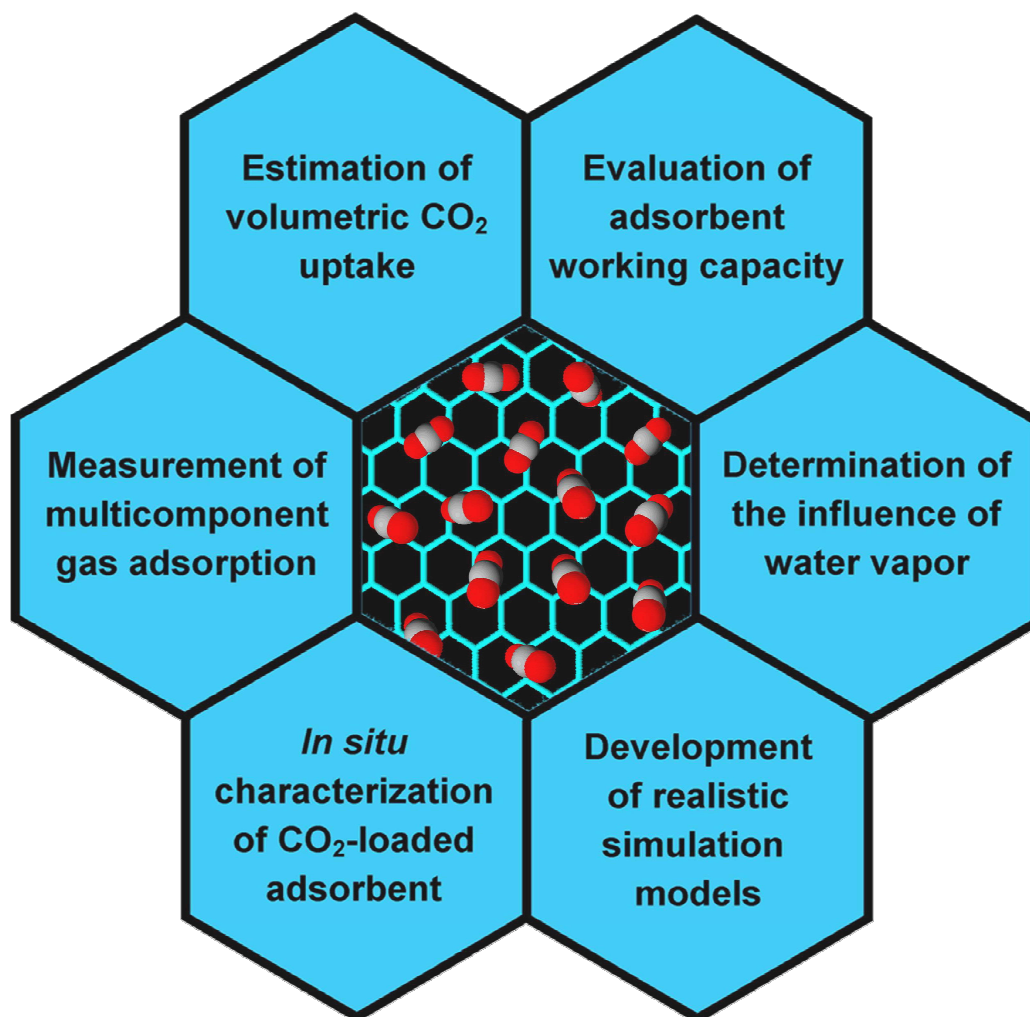
Figure 20

Figure 21

Figure 22

Tables

Table 1 Composition and physical condition of gas streams relevant to pre-combustion and post-combustion CO_2 capture processes.[18-20]

		Pre-combustion capture		Post-combustion capture	
		Gasification fuel gas	Post water-gas shift reaction	Coal-fired flue gas	Natural gas-fired flue gas
Composition	N_2 (vol%)	2—5	2—4	70—80	74—80
	CO_2 (vol%)	1—4	30—40	10—15	3—5
	O_2 (vol%)	—	—	3—4	12—15
	H_2O (vol%)	2—28	6—15	5—10	7—10
	H_2 (vol%)	26—30	40—60	—	—
	CO (vol%)	40—63	<4	<100	<5
	H_2S (ppm)	2000—8000	4000—6000	—	—
	NH_3 (ppm)	50—800	—	—	—
	SO_2 (ppm)	—	—	200—4000	<10
	NO_X (ppm)	—	—	200—800	100—500
	Hg (ppb)	—	—	1—7	—
	Particulate matter (g m^{-3})	8—17	<0.1	5—20	—
Conditions	Temperature (°C)	500—1800	250—550	60—150	~100
	Pressure (bar)	24—70	20—80	~1	~1

Table 2 Physical parameters of gases relevant to CO_2 capture processes.[21]

Gas	Effective kinetic diameter (Å)	Polarizability (10^{-25} cm^{-3})	Dipole moment (10^{-18} esu^{-1} cm^{-1})	Quadrupole moment(10^{-26} esu^{-1} cm^{-1})
N_2	3.64	17.4	0	1.52
CO_2	3.30	29.1	0	4.30
O_2	3.46	15.8	0	0.39
H_2O	2.64	14.5	1.85	—
H_2	2.89	8.0	0	6.62
CO	3.69	19.5	0.12	2.50
H_2S	3.62	37.8—39.5	0.98	—
NO	3.49	17.0	0.16	—
NO_2	—	30.2	0.32	—
SO_2	4.11	37.8—39.5	1.63	—

Table 3 Requisite attributes of an ideal CO_2 adsorbent.[27, 31-34]

Property	Description
High adsorption capacity	Reduces the mass of adsorbent required for a given throughput, lowers the volume of adsorbent bed and minimizes the related equipment size and cost.
High selectivity	High selectivity for CO_2 against other gases ensures that the CO_2 component of the exhaust gas is completely removed for subsequent sequestration.
Moderate heat of adsorption	Heats of adsorption at the borderline between strong physisorption and weak chemisorption provide a good trade-off between selectivity and regeneration.
Fast kinetics	Decreases capital costs, energy requirements for operation and adsorption cycle times.
Chemical/mechanical stability	High chemical stability under the conditions of capture and regeneration maximize adsorbent lifetime and reduce replacement rates to a minimum which has a direct impact on the overall economics of the CO_2 capture process. Good mechanical stability allows the adsorbent to be pulverized into fine particles and densely packed for maximum volumetric capacity. It also warrants that the adsorbent is capable to withstand the bulk handingthat is a feature of any industrial unit.

Table 4 Summary of the experimental results on CO_2 adsorption by graphene-based materials.

Adsorbent	Surface area $(m^2\ g^{-1})^a$	Type of adsorption apparatus	Temp. (°C)	Pressure(bar)	CO_2 uptake $(mmol\ g^{-1})^b$	Isosteric heat of adsorption $(kJ\ mol^{-1})^c$	Selectivity[a]	Ref.
Graphene[d]	639—1550	Volumetric	−78	1	4.8—7.8	—	—	83
Graphene[e]	280—1013	Volumetric	−78	1	2.3—8.6	—	—	83
Graphene[f]	443	Volumetric	25	11	21.6	—	—	84
3D Graphene	477	Volumetric	0	1	0.7	—	—	85
Graphene nanoplate	480	Volumetric	25	30	56.4	—	—	86
Graphene nanomesh	2038	Volumetric	1	31	36.5	—	—	87
HPG[g]	459	Volumetric	0	1	1.8	26	—	88
SAGA[h]	1230	Volumetric	0	1	2.5	—	—	89
PGF[i]	825	Volumetric	−78	0.8	25.5	—	—	90
			0	30.3	9.5	27.4	—	
N-doped graphene[j]	1360	Volumetric	25	1	4.3	—	CO_2/N_2, 34[*]	91
N-doped graphene[k]	980	Volumetric	25	1	2.7	56	CO_2/N_2, 18[*] CO_2/CH_4, 4[*]	92
N-doped graphene[l]	535	Volumetric	25	1	3.0	—	CO_2/N_2, 23[*] CO_2/H_2, 85[*] CO_2/CH_4, 4[*]	93

S-doped graphene	1396	Volumetric	25	1	4.5	—	CO_2/N_2, 51[*] CO_2/H_2, 214[*] CO_2/CH_4, 12[*]	94
B-doped graphene	514	Volumetric	25	1.01	1.8	—	—	95
IL-f-graphene[m]	—	Volumetric	10	1	0.7	21 ± 1	—	96
PIL-f-graphene[n]	—	Volumetric	10	1	0.8	23.5 ± 1	—	96
Graphene/terpyridine	440	Volumetric	0	1	2.7	—	—	97
Graphene/polyaniline	—	Volumetric	25	11	75	—	—	98
Graphene/Fe_3O_4	98	Volumetric	25	11	60	—	—	99
Graphene/Mn_3O_4	541	Volumetric	0	1	2.6	—	—	100
PEI/G-silica[o]	32	Gravimetric	75	7.5	4.3	~100	—	101
Exfoliated GO	547	Volumetric	25	30	6.4	—	—	102
GO-based carbon	1894	Volumetric	27	20	16.4	~21	—	103
GO-based hydrogel	530	Volumetric	0	1	2.4	51	CO_2/N_2, 91[**]	104
GO/TiO_2	100	Volumetric	25	1	1.9	17.5	CO_2/N_2, 22[**]	105
GO/LDH[p]	150 ± 0.35	Gravimetric	300	0.2	0.5 ± 0.02	—	—	106
GO/LDO[q]	116	Gravimetric	300	0.15	0.5	—	—	107
GO/PEI[r]	253 ± 22	Volumetric	0	1	2.5	—	—	108
GO/chitosan	412	Gravimetric	25	1	4.1	~20.5	—	109
GO/DAB[s] (*dry*)	—	Gravimetric	37	1	0.8	—	—	110
GO/DAB (*wet*)					2	—	—	

GO/ZIF-8[t]	289	Volumetric	−78	1.01	16.5	31.9	—	111
GO/Cu-BTC[u]	1677	Volumetric	0	1	8.2	—	CO_2/CH_4, 14[***]	112
GO/MIL-101[v]	2950	Gravimetric	25	25	22.4	45	CO_2/CH_4, 15[***]	113
GO/UiO-66[w]	1184	Volumetric	25	1	3.4	—	—	114
GO-TETA-Ac/Cu$_3$(BTC)$_2$[x]	2043	Volumetric	25	1	5.6	—	CO_2/N_2, 21[**]	115

[a]Values are rounded off to the nearest whole number wherever applicable, [b] Values are rounded off to one decimal place wherever applicable, [c] This datais taken both from single listed values and from plots of heat of adsorption as a function of loading. No attempt is made to distinguish between heat of adsorption and isosteric heat of adsorption. Only one value for each material is taken from each source. If a range or multiple values is reported in the corresponding reference, the initial loading value is used, unless this is not specified in which the highest listed value is preferred,[d]Prepared by thermal exfoliation of GO, [e]Prepared by thermal treatment of nanodiamond, [f]Prepared by hydrogen induced thermal exfoliation of GO, [g]Hierarchical porous graphene,[h]Steam activated graphene aerogel,[i]Porous graphene framework,[j] Prepared by KOH activation of graphene/polypyrrole composite,[k] Prepared by KOHactivation of rGO/polyaniline composite, [l]Prepared by KOH activation of rGO/polyindole composite, [m]Ionic liquid (1-butyl-3-methylimidazolium tetrafluoroborate) functionalized graphene, [n]Polymerized ionic liquid(poly(3-ethyl-1-vinylimidazolium tetrafluoroborate)) functionalized graphene, [o]Polyethyleneimine impregnated graphene-based mesoporous silica sheets,[p]GO/layered double hydroxides, [q]GO/layered double oxides, [r]GO/polyethylenimine,[s]GO/diaminobutanepoly-propylene-iminedendrimer,[t]GO/Zn(2-methylimidazolate)$_2$, [u]GO/copper benzene-1,3,5-tricarboxylate,[v] GO/Cr$_3$O(H$_2$O)$_2$F(1,4-benzenedicarboxylate)$_3$,[w]GO/Zn$_6$O$_4$(OH)$_4$(1,4-benzenedicarboxylate)$_6$, [x]GO-triethylenetetraminetetrafluoroborate/Cu$_3$(1,3,5-benzenetriscarboxylate)$_2$,[*] Calculated using Henry's law, [**]Calculated using single-component gas adsorption isotherm data at low pressure, [***] Calculated using ideal adsorbed solution theory (IAST).

Table 5 Summary of the theoretical studies on CO_2 adsorption by graphene-based materials.

Type of graphene material	Simulation method	Key finding	Ref.
Defective graphene	DFT	Physisorption on defect site and subsequent dissociative chemisorption.	130
Defective graphene	DFT	Stronger physisorption on defective graphene (monovacancy defect) compared with pristine graphene (defect-free).	131
Nanographene	GCMC	Edge sites exhibit greater CO_2/N_2 selectivity than basal planes.	132
Edge-functionalized zigzag graphene nanoribbon	DFT	Functionalization with polar groups strengthens CO_2 binding.	133
Edge-functionalized bilayer graphene nanoribbon	MP2[a] + GCMC	–COOH functionalization enhances both CO_2 adsorption and CO_2/N_2 selectivity.	134
Ti–graphene	DFT + MD[b]	Grafting monodispersed Ti atoms on graphene surface significantly improves CO_2 uptake.	135
Ca-doped graphene	DFT	Ca-doping results in unusually large CO_2 uptake capacities (~0.4―0.6 g CO_2/g adsorbent) and high CO_2/N_2 selectivity.	136

Li-doped graphene	DFT	Li-doping augments CO_2 binding energy and hence the capture potential.	137
Al-doped graphene	DFT	Similar effect to that of Li-doping but more pronounced.	137
Graphene/fullerene	GCMC	CO_2 storage capacity increases with increasing fullerene concentration.	138
Pillared GO framework	DFT + GCMC	CO_2 adsorption varies as a function of the density of pillars and the specific chemical moiety used as spacer; high CO_2/H_2 selectivity at low pressures.	139
Hydrated/Anhydrous GO	DFT	CO_2 desorption from anhydrous GO layers involves lower energy consumption compared with hydrated GO layers.	140

[a] Second-order Møller-Plesset Perturbation Theory, [b] Molecular Dynamics.